

ISSN 1590-8844  
*Vol. 13 No 01*  
2012

# *International Journal of Mechanics and Control*

**Editor: Andrea Manuello Bertetto**



LIBRERIA EDITRICE UNIVERSITARIA  
**LEVROTTO & BELLA**  
TORINO

Editorial Board of the  
***International Journal of Mechanics and Control***

Published by Levrotto&Bella – Torino – Italy E.C.

*Honorary editors*

**Guido Belforte**

**Kazy Yamafuji**

**Editor: Andrea Manuello Bertetto**

**General Secretariat: Elvio Bonisoli**

Atlas Akhmetzyanov  
*V.A.Trapeznikov Institute of Control Sciences  
of Russian Academy of Sciences  
Moscow – Russia*

Domenico Appendino  
*Prima Industrie  
Torino – Italy*

Kenji Araki  
*Saitama University  
Shimo Okubo, Urawa  
Saitama – Japan*

Guido Belforte  
*Technical University – Politecnico di Torino  
Torino – Italy*

Bruno A. Boley  
*Columbia University,  
New York – USA*

Marco Ceccarelli  
*LARM at DIMSAT  
University of Cassino  
Cassino – Italy*

Amalia Ercoli Finzi  
*Technical University – Politecnico di Milano  
Milano – Italy*

Carlo Ferraresi  
*Technical University – Politecnico di Torino  
Torino – Italy*

Anindya Ghoshal  
*Arizona State University  
Tempe – Arizona – USA*

Nunziatino Gualtieri  
*Space System Group  
Alenia Spazio  
Torino – Italy*

Alexandre Ivanov  
*Technical University – Politecnico di Torino  
Torino – Italy*

Giovanni Jacazio  
*Technical University – Politecnico di Torino  
Torino – Italy*

Takashi Kawamura  
*Shinshu University  
Nagano – Japan*

Kin Huat Low  
*School of Mechanical and Aerospace Engineering  
Nanyang Technological University  
Singapore*

Andrea Manuello Bertetto  
*University of Cagliari  
Cagliari – Italy*

Stamos Papastergiou  
*Jet Joint Undertaking  
Abingdon – United Kingdom*

Mihailo Ristic  
*Imperial College  
London – United Kingdom*

János Somló  
*Technical University of Budapest  
Budapest – Hungary*

Jozef Suchy  
*Faculty of Natural Science  
Banska Bystrica – Slovakia*

Federico Thomas  
*Instituto de Robótica e Informática Industrial  
(CSIC-UPC)  
Barcelona – Espana*

Lubomir Uher  
*Institute of Control Theory and Robotics  
Bratislava – Slovakia*

Furio Vatta  
*Technical University – Politecnico di Torino  
Torino – Italy*

Vladimir Viktorov  
*Technical University – Politecnico di Torino  
Torino – Italy*

Kazy Yamafuji  
*University of Electro-Communications  
Tokyo – Japan*

*Official Torino Italy Court Registration  
n.5390, 5<sup>th</sup> May 2000*

*Deposito presso il Tribunale di Torino  
numero 5390 del 5 maggio 2000*

*Direttore responsabile:*

*Andrea Manuello Bertetto*

# ***International Journal of Mechanics and Control***

***Editor: Andrea Manuello Bertetto***

***Honorary editors: Guido Belforte  
Kazy Yamafuji***

***General Secretariat: Elvio Bonisoli***

The Journal is addressed to scientists and engineers who work in the fields of mechanics (mechanics, machines, systems, control, structures). It is edited in Turin (Northern Italy) by Levrotto&Bella Co., with an international board of editors. It will have not advertising.

Turin has a great and long tradition in mechanics and automation of mechanical systems. The journal would will to satisfy the needs of young research workers of having their work published on a qualified paper in a short time, and of the public need to read the results of researches as fast as possible.

Interested parties will be University Departments, Private or Public Research Centres, Innovative Industries.

## ***Aims and scope***

The *International Journal of Mechanics and Control* publishes as rapidly as possible manuscripts of high standards. It aims at providing a fast means of exchange of ideas among workers in Mechanics, at offering an effective method of bringing new results quickly to the public and at establishing an informal vehicle for the discussion of ideas that may still in the formative stages.

## ***Language: English***

*International Journal of Mechanics and Control* will publish both scientific and applied contributions. The scope of the journal includes theoretical and computational methods, their applications and experimental procedures used to validate the theoretical foundations. The research reported in the journal will address the issues of new formulations, solution, algorithms, computational efficiency, analytical and computational kinematics synthesis, system dynamics, structures, flexibility effects, control, optimisation, real-time simulation, reliability and durability. Fields such as vehicle dynamics, aerospace technology, robotics and mechatronics, machine dynamics, crashworthiness, biomechanics, computer graphics, or system identification are also covered by the journal.

*Please address contributions to*

Prof. Guido Belforte  
Prof. Andrea Manuello Bertetto  
PhD Eng. Elvio Bonisoli

*Dept. of Mechanics  
Technical University - Politecnico di Torino  
C.so Duca degli Abruzzi, 24.  
10129 - Torino - Italy - E.C.*

www.jomac.it  
e\_mail: jomac@polito.it

## *Subscription information*

Subscription order must be sent to the publisher:

*Libreria Editrice Universitaria  
Levrotto&Bella  
2/E via Pigafetta – 10129 Torino – Italy*

www.levrotto-bella.net  
e\_mail: info@levrotto-bella.net  
tel. +39.011.5097367  
+39.011.5083690  
fax +39.011.504025



# A PTZ STEREO CAMERA VISION SYSTEM FOR ROBOTIC PERCEPTION

Gigel Macesanu      Sorin Mihai Grigorescu      Florin Moldoveanu

Department of Automation, Transilvania University of Brasov, Romania

## ABSTRACT

In robotics, the most common approach to 3D reconstruction and scene understanding is through stereo vision. In order to keep track the 3D *positions* and *orientations* (pose) of objects of interest over a large Field of View (FOV), the orientations and focal lengths of the stereo camera system must be adjusted, that is, the pan, tilt and zoom (PTZ) of both vision sensors. In this paper the practical implementation of a 3D object reconstruction and tracking system, using two PTZ cameras in a stereo configuration, is presented. Firstly, the stereo platform is calibrated and the intrinsic and extrinsic parameters of the sensors determined. Secondly, the 2D image streams are processed in order to segment and classify the objects present in the environment. Based on the implemented methods, the objects of interest can be reconstructed in a virtual 3D space through the epipolar geometry constraints. The feedback mechanism for controlling the orientation and zoom of the two cameras are derived directly from the 3D poses of the objects of interest. As performance evaluation, we present a stability analysis of the proposed active vision system, taking into account the time-delay introduced by the image processing system.

Keywords: PTZ control, active vision, 3D reconstruction, stability analysis

## 1 INTRODUCTION

Conventional robot vision systems use stereo cameras with a fixed orientation and zoom, this fact leading to physical limitations in the scene understanding process. In situation in which non stationary objects should be observed and tracked, the fixed cameras are replaced with systems that able to adapt their viewpoint and zoom along with the poses of the objects. Thus, the visual perceptual capabilities of an autonomous robot are adapted according to the imaged environment, evaluating the camera's extrinsic parameters (i.e. pose and zoom) modifications. Using such an *active vision system*, a robotic platform can track objects of interest and reconstruct their poses in a virtual 3D space.

The accuracy of a robotic platform depends directly on the accuracy of the visual sensor. An alternative to increasing the accuracy of these subsystems, that is, of the vision sensors is to use a *visual-feedback control loop*. The concept of visual feedback control has been heavily investigated in the computer vision community [7], [15].

The idea of using such feedback information at the image processing level can be found in older papers such as [14] where the effect of video feedback is described for robotic positioning tasks. This process, in which the visual data is used to control robotic platforms, is also encountered under the name of *visual servoing* [3].

In literature, there are a number of 3D object reconstruction methods, which can be classified into two different groups [6]: active and passive methods. The active methods use laser, or structured light systems, to obtain 3D data. The passive methods approaches use digital cameras which acquire images from different points of view. The main advantages of using the passive approach are related to the acquisition price and the operation simplicity. The 3D reconstruction model is constructed using the triangulation method, which represents the process of finding coordinates of a 3D point based on its corresponding stereo

---

Contact authors: G. Macesanu<sup>1</sup>, S.M. Grigorescu<sup>2</sup>,  
F. Moldoveanu<sup>3</sup>

<sup>1</sup>Email: [gigel.macesanu@unitbv.ro](mailto:gigel.macesanu@unitbv.ro)

<sup>2</sup>Email: [s.grigorescu@unitbv.ro](mailto:s.grigorescu@unitbv.ro)

<sup>3</sup>Email: [moldof@unitbv.ro](mailto:moldof@unitbv.ro)

URL: [www.rovis.unitbv.ro](http://www.rovis.unitbv.ro)

image points, as well as with the intrinsic parameters of the cameras (e.g. *focal length*, *optical center*, etc.) [4].

The main goal of the research presented in this paper is to reconstruct a 3D scene using the information acquired from a stereo camera system and to automatically adapt the orientation of the stereo camera according to the pose of the imaged object of interest. The resulted 3D model can be used by an autonomous robot to navigate in unknown environments, avoid obstacles, or grasp objects if the robot is equipped with a redundant manipulator. In this paper we also propose a stability analysis of the active stereo vision architecture, taking into account the time-delay introduced by the image processing software.

The rest of the paper is organized as follows. In Section II, the stereo camera calibration and image rectification process are presented. The camera control system is described in Section III, followed in Section IV by the overall system stability analysis. Finally, conclusions are stated in Section V.

## 2 STEREO CAMERA CALIBRATION AND RECTIFICATION

One important problem to be solved in obtaining the position of an object of interest is the estimation of the distance between the camera and the object. This distance is determined using a calibrated stereo camera. In order to determine the object's 3D position, the images used must be rectified.

### 2.1 STEREO GEOMETRY

The standard model of a stereo camera is illustrated in Figure 1 [9]. A real world point  $P(x, y, z)$  is projected onto the image planes of a stereo camera as the homogeneous 2D image points:

$$\begin{cases} p_l = (x_l, y_l, 1), \\ p_r = (x_r, y_r, 1), \end{cases} \quad (1)$$

where,  $p_l$  and  $p_r$  represents the projection of a  $P$  point

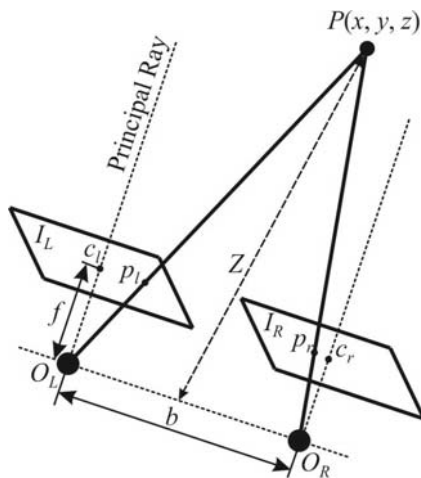


Figure 1 Stereo camera geometry.

which has the  $(x_l, y_l)$  and  $(x_r, y_r)$  coordinates. The projected points are situated on the left  $I_L$  and right  $I_R$  images, respectively. The  $O_L$  and  $O_R$  represent the camera's optical centers. The plane formed by the optical centers and the  $P$  point represents the epipolar plane. This plane intersects the image plane in  $p_l$  and  $p_r$ .

The image, or the principal plane, is located at a distance  $f$  from the optical center of the camera, where  $f$  is the focal length. The  $z$  axis of the coordinate system attached to the optical center is referred to as the principal ray, or optical axis. The intersection between the image plane and the principal ray at the image center is known as the principal point,  $c_l$  and  $c_r$ . In order to determine the distance  $Z$  from the stereo camera to point  $P$  the distance  $b$  between the optical centers of the two cameras and the projection points  $p_l$  and  $p_r$  has to be known. Knowing these parameters, the 3D position of  $P$  with respect to the camera can be obtained. The 3D position of  $P$  is determined using the following equations [10]:

$$x = x_l \cdot \frac{b}{d}, \quad (2)$$

$$y = y_l \cdot \frac{b}{d}, \quad (3)$$

$$z = f \cdot \frac{b}{d}, \quad (4)$$

where,  $d$  represent the disparity of the projected point  $P$  and is equal with:

$$d = x_l - y_r \quad (5)$$

Using the above equations we are able to compute the 3D position of a point, based on its 2D Cartesian position and camera parameters.

### 2.2 STEREO CALIBRATION AND RECTIFICATION

The process of stereo camera calibration is supposed to determine the internal and external camera parameters. The internal parameters, that is *intrinsic parameters*, are obtained based on the Zang method [16]. The resulted intrinsic calibration matrix has the follow form:

$$K = \begin{vmatrix} f_x & 0 & c_x \\ 0 & f_y & c_y \\ 0 & 0 & 1 \end{vmatrix}, \quad (6)$$

where,  $f_x$  and  $f_y$  are the horizontal and vertical camera's focal length, whereas  $c_x$  and  $c_y$  are the focal points.

Other computed parameters are the distortion coefficients. In this case we compute two types of distortions: *radial* and *tangential*. Radial distortions appear as a result of the shape of lens, whereas tangential distortions arise from the assembly process of the camera. These parameters are computed using the method proposed by Brown [2].

While the above parameters are specific for each camera, and contain internal camera's specifications, the extrinsic

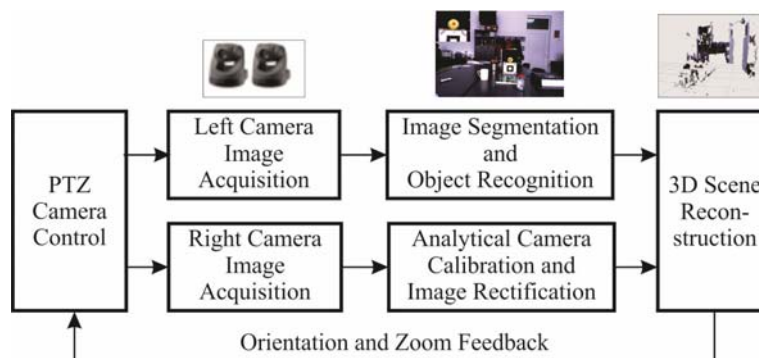


Figure 2 The architecture of the stereo control system.

parameters show the relative position of the cameras. The extrinsic parameters contain two vectors: rotation and translation and has the form:

$$E = \begin{bmatrix} R_{3 \times 3} & T_{3 \times 1} \\ 0_{1 \times 3} & 1 \end{bmatrix}, \quad (7)$$

where,  $R_{3 \times 3}$  represent the rotation matrix and  $T_{3 \times 1}$  is the translation matrix. These vectors contain the position of the left camera relatively to the right camera. First parameters of the translation vector are represented by the cameras baseline  $b$  (see Figure 1).

In our implementation we calculate the intrinsic and extrinsic matrices using a calibration chessboard table, imaged in a number of 25 frames.

The rectification process transforms each image plain in such a way that pairs of conjugate epipolar lines become collinear and parallel to one of the image axes. This process is needed because the real stereo system isn't perfectly aligned, since the two cameras almost never have exactly coplanar, row-aligned imaging planes.

The process of rectification is realized based on the simplified method developed by Zhang [16] who use only the rotation matrix,  $R_{3 \times 3}$ , and the translation matrix,  $T_{3 \times 1}$ , obtained from the calibration process. The returned values from the rectification process include two matrices that rotate the left camera about the center of projection so that the position of epipols to be at infinity and the epipolar line becomes horizontal (see Figure 1) [1].

### 2.3 STEREO CORRESPONDENCES

Another important process in scene reconstruction is represented by the correspondences problem. The idea is to find the same point from the left image into the right images. If the camera geometry is known, the correspondence problem is reduced to the fact that points in one image can correspond only to points along the same scan-line in the other image [12].

Thus, using the geometry resulted from the calibration process and the rectified images we can compute correspondences between the two views.

In this paper, the method of *Block Matching* (BM) has been used for estimating camera-objects distances. The block matching algorithm is based on using small windows to find matching points between the left and the right rectified stereo images. The match is based by computing a *Sum of Absolute Differences* (SAD) [11]. This algorithm is used for measuring the similarity between image blocks and works by computing the absolute difference between each pixel in the original block and the corresponding pixel in the block being used for comparison.

The process of block matching using SAD can be divided into three distinct stages:

- *pre-filtering* – the input images are normalized, in order to enhance textures and to reduce lighting differences, these are done by using a  $7 \times 7$  window;
- *correspondence matching* – in this stage are search correspondences using a sliding SAD window. The search is done along the horizontal epipolar lines;
- *post-filtering* – represent the process of eliminate bad correspondences matches.

The BM algorithm is applied on rectified images, thus, correspondences are search along the same row in both images of the stereo pair. The interval in which the correspondent point is search has a finite distance, with its low value called *minimum disparity*, while it's high value is named *maximum disparity*. The interval between the minimum and maximum value is the so-called *horopter*, defined as the 3D volume that is covered by the search range of the stereo algorithm [4], [1].

### 3 STEREO CAMERA CONTROL

The block diagram of the proposed stereo control architecture is presented in Figure 2. The robotic head is composed from two digital Pan-Tilt-Zoom cameras which compose the artificial vision system. Based on these cameras, stereo images are acquired and used for analytical stereo calibration and image rectification. At the same time images are used for object recognition. Both results, calibration with rectification and object recognition are used as inputs for the 3D scene reconstruction.

### 3.1 2D OBJECT RECOGNITION

The process of object of interest detection begins with an images filtering. The process of filtering involves the shifting of a filter mask,  $w(i, j)$  over the input image. At each point  $(x, y)$ , the response of the filter at that point is calculated using a predefined relationship [8]. In our implementation a 3x3 mask was used. The object of interest is detected using color segmentation. This involves a color representation conversion, from RGB (*Red, Green, Blue*) format to HSI (*Hue, Saturation, Intensity*) color model.

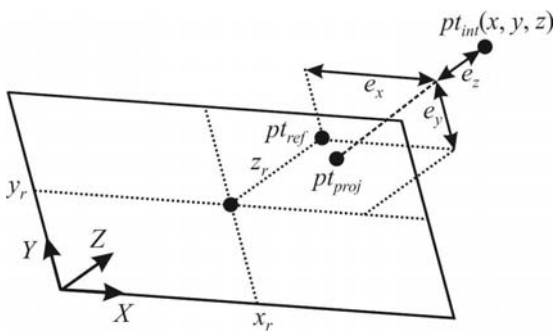


Figure 3 The position error for a 3D point.

Using the conversion other colors than the desired are rejected. The segmentation process is followed by the detection of the object's contour in the 2D image plane using the chain-code border following method [1].

The object of interest contour recognition is performed using invariant Hu moments that are invariant to object rotation, translation and scaling. Using the coordinates of the central of gravity for each object, detected in the left and the right image and the epipolar geometry, presented in previous section, we are able to reconstruct the 3D position of the object. Using the 3D position of an object of interest we can perform an active vision control that involves sending back to the PTZ camera control, as feedback information, the current object position.

This fact leads to adapting the cameras parameters in such a way to obtain an optimal visualization. Using only the correspondent points, extracted from the block matching algorithm, we can reconstruct the whole viewed scene. This robotic active vision system can perform an object of interest proper visualization and whole scene reconstruction.

### 3.2 CAMERA ORIENTATION SYSTEM

During the robot navigation the position of the objects of interest can change. The goal of the proposed active vision system is to maintain the image object in the middle of the 2D image plane, as well as within the image boundaries. These conditions can be satisfied using a system with the camera's *Field of View* (FOV) automatically adjustable, in order to cover a wider scene as possible. The scene where the position of the objects of interest can be too far or too

close from the vision sensor can't be analysed using conventional pan and tilt cameras. This problem can be solved by adding an extra *Degree of Freedom* (DoF) to the camera, that is, of the zoom control system. This extra control system aims at controlling the focal length through with the environment is sensed.

The active vision system has to minimize three errors, one for each axis of the coordinate system. The errors which have to be compensated by the active vision system are illustrated in Figure 3, where the position of a real world point,  $pt_{int}(x, y, z)$  in the 3D Cartesian space, along with its 2D location in the image plane  $pt_{proj}(x, y)$  is presented. The 3D point  $pt_{ref}(x_r, y_r, z_r)$  represents the reference (desired) position for the object of interest position. The  $x_r$  and  $y_r$  coordinates represent the 2D central coordinates, while the  $z_r$  is the distance, or depth, from the middle point on the baseline between the two cameras and the imaged object.

The position error can be defined as the difference between the current position of the objects of interest in 3D space and the reference position:

$$e = pt_{int} - pt_{ref}, \quad (8)$$

where,  $e = |e_x, e_y, e_z|$ , represent the position error vector,  $pt_{int}(x, y, z)$  and  $pt_{ref}(x_r, y_r, z_r)$  represent the real position and the desired position of the object of interest. The goal of the visual controller is to minimize the  $e_x$  and  $e_y$  errors by adjusting the pan and tilt values of the cameras and  $e_z$  by controlling the focal length of the cameras.

## 4 STABILITY ANALYSIS

To evaluate the performance of the system we analyse the stability of the proposed control structure. The analysis supposed to study all three moving elements: pan, tilt and zoom. Because all of them are identical as structure, only their role in the system is different, we analyse only the pan (the other two are identical). In this sense we have used the *Nyquist criterion* with the gain margin  $k_g$  and phase margin  $\gamma$  for the frequency response method [5].

In the Nyquist criterion, the locus of open-loop transfer function represents a measure of the system's relative stability. The objective of this analysis it to determine the gain and phase margins in order to observe the system's stability reserve.

The open-loop transfer function, in the frequency domain of the active vision system, with its block diagram presented in Figure 4, is defined as:

$$G(j\omega) = \frac{1.7}{1 + 0.24j\omega} \cdot e^{-s\tau}, \quad (9)$$

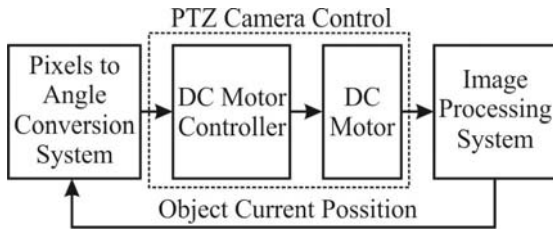


Figure 4 Block diagram of the active control system.

where,  $\tau$  represent the time-delay introduced by the image processing component [3]. The transfer function is composed from a DC (direct current) motor with its controller and an additional controller for pixels to angles conversions. The DC and its controller are modelled as *first order lag element* (PT1) and the conversion system as a *proportional element* (P). The parameters of the controllers were chosen in order to obtain a zero steady-state error and an optimal rise time.

The analysis is performed in an open-loop loop manner on the transfer function, without considering the time-delay. The goal of the approach is to determine the open-loop stability and to observe the closed-loop system's evolution when a time-delay is introduced. For this purpose, the phase margin and its associated gain crossover frequency has to be determined.

The gain crossover frequency is determined using the following equation:

$$|G^*(j\omega_g)| = 1, \quad (10)$$

where,  $G^*(j\omega_g)$  represent the open-loop transfer function without time-delay and  $\omega_g$  represent the gain crossover frequency. After solving the above equation, a value of  $\omega_g = 5.728$  is obtained.

The phase margin for the time-delay free open-loop transfer function can be written as:

$$\begin{aligned} \gamma &= 180^\circ + \arg(G^*(j\omega_g)) = \\ &= 180^\circ - \arctg(\omega_g \cdot 0.24) = 126.1^\circ \end{aligned} \quad (11)$$

When a time-delay exists within the system, it affects the phase margin and its associated frequency. The phase margin is the amount of additional phase lag, at the gain crossover frequency, which can bring the system to the stability limit [13], can be computed as:

$$180^\circ + \arg(G^*(j\omega_g)) - \omega_g \cdot \tau, \quad (12)$$

where  $\tau$  represent the time-delay.

When the system is at stability limit, the time-delay phase margin is zero:

$$180^\circ + \arg(G^*(j\omega_g)) - \omega_g \cdot \tau = 0. \quad (13)$$

Using the previously equations we can determine the maximum value of the time-delay,  $\tau_{\max}$  after which the overall closed-loop system becomes unstable:

$$\tau_{\max} = \frac{[180^\circ + \arg(G^*(j\omega_g))]_{rad}}{\omega_g} = 0.38 \text{sec} \quad (14)$$

The obtained maximum values of time-delay Eq. (14) indicates that the image processing chain from Figure 2 should process a pair of stereo images (e.g. image acquisition, segmentation, object recognition and 3D reconstruction) in less than 0.38sec.

## 5 EXPERIMENTAL RESULTS

The stereo acquisition system is composed of two Sony PTZ cameras, which was placed at 1.4m above the ground. The cameras acquire images with a resolution of 640x480 pixels. The system reacts when an object of interest appears inside the camera's field of view. The tennis ball (which is used as object of interest), is moved by a human person in a random pose. The commands values for pan/tilt movements and the real pose obtained from cameras encoders are saved on a remote computer. The experiments were performed in an indoor room, using artificial illumination. The ball was moved inside the room, covering an area of about 9m<sup>2</sup>.

During the experiments the mean error was computed, while the camera was performing a movement between [-40°, 60°] for pan and a movement between [-10°, 45°] for tilt. The error is computed using the following expression:

$$er[\text{deg}] = pos_{est} - pos_{real} \quad (15)$$

where,  $er$  represents the error in degree,  $pos_{est}$  represents the position used as command and  $pos_{real}$  represents the position read from cameras encoders.

In Figure 5 (a,b) are presented the real pan angle and the command values used to control the pan and tilt angle of a stereo camera. The obtained errors when the camera is moving with 50°/sec are summarized in table I.

Table I - Position errors for pan and tilt movements.

Item	Mean error
Pan left	4.607
Pan right	7.277
Tilt left	3.342
Tilt Right	2.085

## 5. CONCLUSION

This paper presents an active stereo vision system for autonomous robots which have to sense the 3D structure of the images environment. The presented algorithms aim at detecting the 2D location of the object of interest in the image plane and at reconstructing their pose in a virtual 3D space. Based on the obtained 3D model the orientation of the camera system can be automatically adapted. The stability of the proposed system is investigated based on the time-delay introduced by the image processing software.

## 6. ACKNOWLEDGMENTS

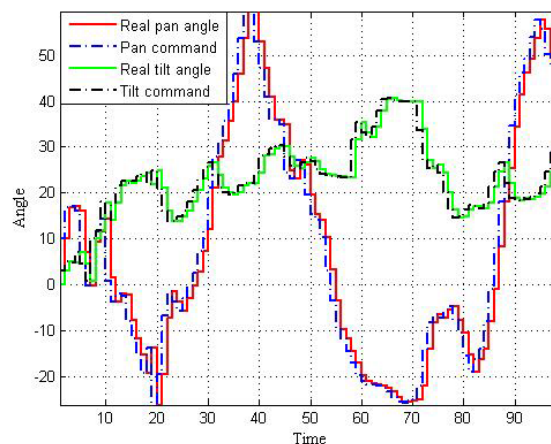
This paper is supported by the Sectoral Operational Programme Human Resources Development (SOP HRD), financed from the European Social Fund and by the Romanian Government under the contracts number POSDRU/88/1.5/S/59321, POSDRU/89/1.5/S/59323.

## REFERENCES

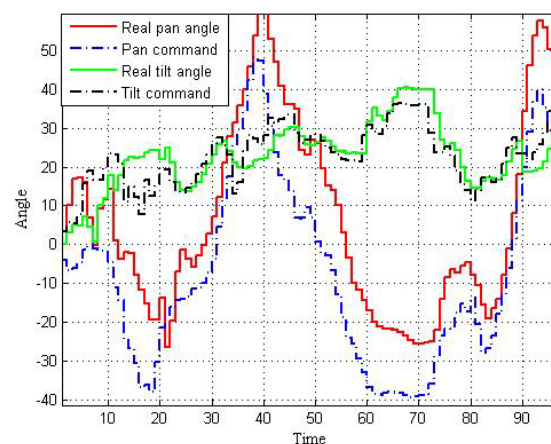
- [1] Bradski G. and Kaehler A., *Learning OpenCV*. O'Reilly Media, Sebastopol, USA, 2008.
- [2] Brown D.C., Close-range camera calibration. *Photogrammetric Engineering*, Vol. 37, No. 1. pp. 855–866, 1971.
- [3] Corke P.I., *Visual Control of Robots: A High-performance Visual Servoing*. Research Studies Press Ltd., John Wiley & Sons Inc, Great Britain, 1996.
- [4] Cyganek B. and Siebert J.P., *An Introduction to 3D Computer Vision Techniques and Algorithms*. John Wiley & Sons, Great Britain, 2009.
- [5] Dorf R.C. and Bishop R.H., *Modern Control Systems*, 12th edition. Prentice Hall, New Jersey, USA, 2010.
- [6] Esteban C.H. and Schmitt F., Silhouette and Stereo Fusion for 3D Object Modeling. *Computer Vision and Image Understanding*, Vol. 96, No.2, pp. 367-392, 2004.
- [7] Fitzpatrick P., First Contact: an Active Vision Approach to Segmentation. *Proc. Of the 2003 IEEE/RSJ Int. Conf. on Intelligent Robots and Systems*, Las Vegas, USA, pp. 2161-2166, 2003.
- [8] Gonzalez R.C. and Woods R.E., *Digital Image Processing*, 2nd edition. Prentice Hall, New Jersey, USA, 2002.
- [9] Hartley R. and Zisserman A., *Multiple View Geometry in Computer Vision*, 2nd edition, Cambridge University Press, Cambridge, United Kingdom, 2004.
- [10] Huang Y., Fu S. and Thompson C., Stereovision-Based Object Segmentation for Automotive Applications. *EURASIP Journal on Applied Signal Processing*, Vol. 2005, No. 14, pp. 2322–2329, 2005.
- [11] Kisacanin B., Bhattacharyya S.S. and Chai S., *Embedded Computer Vision*. Springer-Verlag, London, United Kingdom, 2009.
- [12] Ogale A.S. and Kinematics Y.A, Shape and the stereo correspondence problem. *Int. Journal of Computer Vision*, Vol. 65, No. 3, pp. 147-162, 2005.
- [13] Ogata K., *Modern Control Engineering*, 4th edition. Prentice Hall, New Jersey, USA, 2002.
- [14] Shirai Y. and Inoue H., Guiding a Robot by Visual Feedback in Assembling Tasks. *Pattern Recognition*. Vol. 5, pp. 99-108, 1973.
- [15] Welke K., Tamim A. and Dillmann R., Active Multi-View Object Search on a Humanoid Head. *2009 IEEE*

*International Conference on Robotics and Automation*, Kobe, Japan, pp. 417-423, 2009.

- [16] Zhang Z., A Flexible New Technique for Camera Calibration. *IEEE Trans. on Pattern Analysis and Machine Intelligence*, Vol. 22, No. 11, pp.1330-1334, 2000.



(a)



(b)

Figure 5 Active tennis ball tracking system, performance evaluation.

# MECHANICAL HARVESTER AND DOUBLE FLOW CICLONE SEPARATOR: PROTOTYPES TO IMPROVE SAFFRON SPICE PRODUCTIONS

Andrea Manuello Bertetto\*

Roberto Ricciu\*\*

\* Dipartimento di Ingegneria Meccanica, Chimica e dei Materiali

Università degli Studi di Cagliari

\*\* Dipartimento di Ingegneria Civile, Ambientale e Architettura

Università degli Studi di Cagliari

## ABSTRACT

In the Saffron spice production, actually hand made, the harvesting phase and stigma separation would greatly benefit from a mechanization. This paper is concerned with the design and characterization of a saffron flower harvesting and spice separation mechanized system, that system is a workable integrated system to obtain the spice for drying and packaging final phases of spice production. The main parts of the system are represented by a harvesting portable device and a double flow three way cyclone separator. The mechanical operating principle of the harvesting portable device and the working way of the double flow three way cyclone are described. Experimental characterisation illustrates in the paper the mechanical and fluid dynamics behaviour of harvesting and separating devices.

Keywords: automated harvesting, portable robotic device, fluidic separation

## 1 INTRODUCTION

Developing a mechanical system, for the handling of delicate and soft objects as fruits and agricultural products in general, requires to address particular topics as development of robust and dexterous grippers using also non conventional working principle. In the Saffron spice production process, the harvesting and the spice separation are the two most hard phases. Many harvester and separator device are proposed in literature. In particular in agricultural field grippers and cyclone devices are often efficient and gainful. One of the major topics is the design of a proper gripping device to handle delicate objects, such as soft fruits. Saffron morphology involves high attention to the robotic designer because of the presence of different elements which are foils, petals, anthers with the stigmas representing the wanted spice.

This act imposes a particular attention to design the grippers and separators treating objects having different masses, geometries and sizes. For picking delicate objects, many applications employ the vacuum principle to perform a delicate gripping phase. Particular versatility characteristics are required given the necessity of grasping objects of not uniform size and shape which are not located in given known position. For example in [1, 2] a hand is proposed for the automatic harvesting of asparagus in field. A soft hand for delicate fruit harvesting, with pneumatically driven flexible fingers has been developed in [3]. This hand is capable of adapting itself to the object location and size. The yield is very high in the case of flowers to produce spices like Saffron [4, 5].

The cyclone multi-flow device, here designed, refers its working principle to fluidic elements like vortex valves. The author think that these devices offers more degrees of freedom to the flow control to separate selectively the floating objects [6-9].

---

Contact authors: Andrea Manuello Bertetto<sup>1</sup>,

Roberto Ricciu<sup>2</sup>

<sup>1</sup>Piazza d'Armi, 1, 09123 Cagliari - Italy

<sup>2</sup>Via Santa Croce 67, 09124 Cagliari - Italy

## 2 THE HARVESTING DEVICE

The *Crocus Sativus*, as represented in Figure 1, is a specie of *Crocus* among the Iridaceae. *Crocus Sativus* flower bears the stigmas. The flower in the field is about 150mm height and the open flower is about 50mm large. From the stigmas, that are three and with a bright red colour, is derived the spice. Saffron is certainly the world's most expensive spice by weight [10]. Despite the high number of mechanical and robotic machines, introduced in the agricultural field, the harvesting of flowers is not so much automated, not many devices exist for harvesting the really delicate Iridaceae, the family which the saffron belongs.

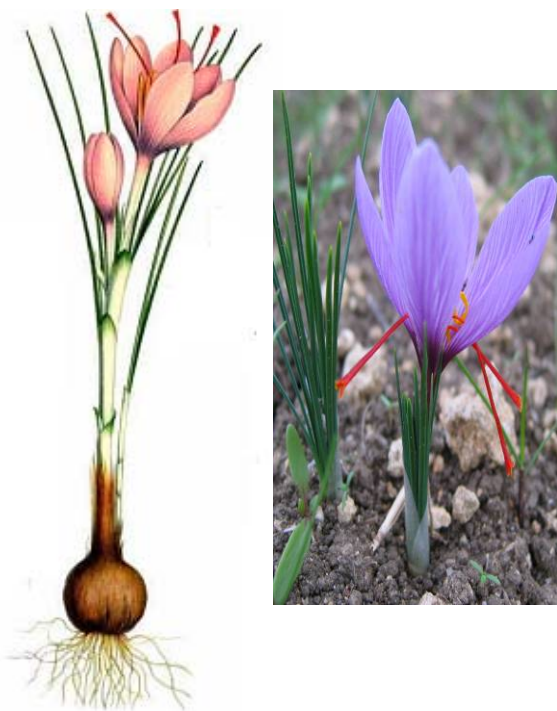


Figure 1 The Saffron flower

The mechanical system described in this paper is concerned about a shoulder portable device with two main parts, the first of which for detaching the corolla from the stem and the second for collecting the flower in a holder.

In Figure 2 the portable device for harvesting *Crocus Sativus* in the field is represented. The device is a lightweight system that make it possible to perform an efficient harvesting operation in the field.

In the figure it can be seen the gripper with two fingers to detach flowers, the body, including the electric motor moving a fan to inhales the detached flowers through the vacuum tube, the handle equipped with a manually operated pneumatic valve to control the pneumatic gripper. The gripper is a one degree of freedom pneumatically actuated device: this kind of power supply is quite suitable for operation in agricultural fields. The success of the detaching phase of the Saffron flower harvesting process is strongly dependent on the dynamics of the system.

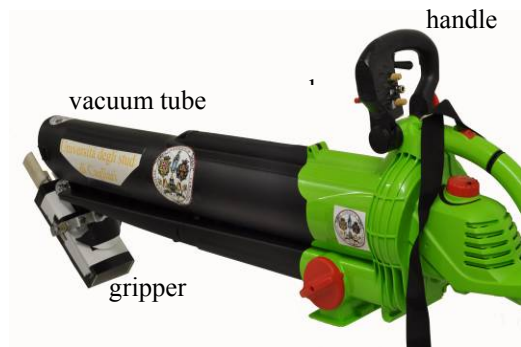


Figure 2 The harvesting device

In Figure 3 the sensorized gripper is shown. In the same figure it can be seen the two fingers powered by the mini pneumatic cylinder, moving an helical cam to convert the translating cylinder rod motion in the helical one of the fingers. Two pressure transducer detects the pressure values in the two cylinder chambers, and a wire position transducer allows to know the cylinder rod position linked to the gripper fingers. The pressure transducers have a range of  $\pm 1.46 \times 10^6$  Pa and a sensitivity of  $6.89 \times 10^3$  Pa/mV; the wire displacement sensor has a 140mm range and a gain of 78.7 mV/mm.

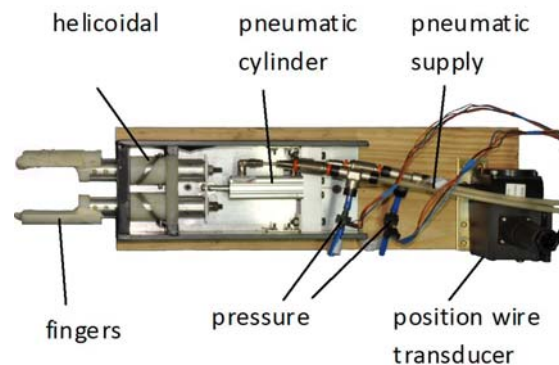


Figure 3 The sensorized gripper on the test rig

The tests here referred are for a supply pressure of 4 bar relative. This pressure level is adequate to perform dynamic behaviour of the gripper during the detaching phase. The graph in Figure 4 refers the rod position and velocity trend vs. the pressure value in the powered cylinder chamber. The rod position is detected by a wire position transducer. The pressure value, when the chamber is discharged, has a trend quickly reaching the environment pressure level, also favoured by the decreasing volume for the piston movement. On the contrary, when the chamber is supplied, the volume increases because of the piston motion and the pressure trend is more gradual. In Figure 4 the stroke and velocity of the rod vs. pressure value in supplied posterior cylinder chamber during the rod coming out phase.

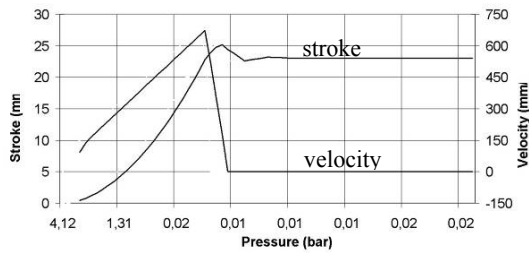


Figure 4 The rod stroke and velocity vs. air relative pressure value in the posterior cylinder chamber, during the rod coming out phase.

For a given supply pressure of 4 bar relative, the maximum velocity value of the cylinder rod is 0.65m/s reached in 0.06 seconds; this corresponds to a medium acceleration of about  $10\text{m/s}^2$ . The dynamic behaviour, strongly dependent on the supply pressure level, is responsible for the success of the harvesting operation. A test procedure was tuned in order to detect the kinematics and dynamic performance without hardware assembly of sensors on board. The gripper behaviour was then also studied by an image analysis technique. This procedure allows an easy portability of the experimental set up to test the gripper behaviour on field during the harvesting phase on field.

In the graph in Figure 5 the cylinder rod position is referred comparing the values detected by the wire position transducer (a) and by optical system (b). By the image analysis technique, it is possible to detect the displacement and velocity of the gripper fingers without an invasive assembly of the transducers. Ten cycles of the piston were recorded at 1000 fps by means of a high speed camera (Redlake Motionpro Y3) with CMOS sensor and a resolution of 1024 x 1280 pixels, equipped with a professional 50 mm lens. The trend difference between the curves (a) and (b) comes from the measurement way. In particular, in the curve (a) it can be seen an overshoot probably due to the measurement system non null mass with a strong deceleration at the end of the stroke. On the contrary, in (b) curve, there is not overshoot because of the optical measurement system doesn't have accelerated significant masses. However, an high frequency oscillation is detected coming from the dynamic of the target linked to the cylinder rod.

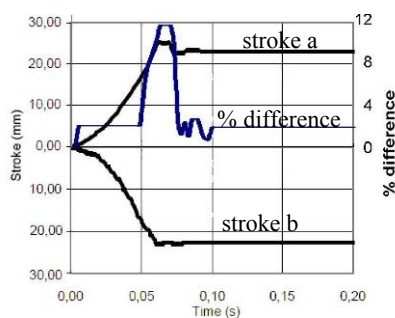


Figure 5 The rod cylinder displacement detected by wire position transducer and by optical way

The harvesting device was tested taking part in field picking Saffron flowers. In Figure 6 the device is shown in open fields in San Gavino Monreale in Sardinia island (Italy). In the photograph it can be seen the device during the grasping phase: the particular way chosen to detach the Saffron flower allows to work on the complete flower with the foils, avoiding to damage them, obtaining the flower detaching in any case.



Figure 6 The harvesting device on field.

In table 1 refers the working condition during the tests on field. In the table are cited four fingers types with covering of different softness. The supply pressure allows an adequate dynamic of the fingers motion, the harvesting times are one-tenth second of magnitude. In the table are also referred the wind velocity, important because of the aerodynamic surface and the light weight of the flowers. One of the test was done in presence of a light rain.

Table I - Working conditions during tests in field

finger type	% Success at the first detaching	detaching time (s)	supply pressure (bar)	wind velocity Beaufort number	rain
type 1	80%	0,2	4,0	1 20 km/h	no
type 2	70%	0,2	4.0	3 15 km/h	no
type 1	95%	0,2	4.5	3 15 km/h	light
type 4	75%	0,2	5.0	0 0 km/h	no

In Figure 7 the flowers detached by the harvesting device are represented.



Figure 7 The flowers detached by the harvesting device

It can be noted that the detached flowers are undamaged by the grasping and detaching procedure. In particular, the spice, represented by three red stigmas, is in its place in the goblet not damaged by the mechanised harvesting. The stems are broken correctly, avoiding to damage bulbs and foils.

### 3 THE SEPARATOR

The working phase of the Saffron spice production are four: harvesting, spice separation, drying and packaging. The most heavy are the harvesting and separation phases. Regarding to the separation phase the operation is actually strictly manual, long and expensive. In this work, the authors show a particular type of cyclone separator, having two inlet flows and one exit port. This kind of fluidic device refers its architecture to a particular device able to regulate flows avoiding mobile mechanical parts: the vortex valve are used in plants with very high security and safe requirements.

In Figure 8 a vortex valve and double flow cyclone scheme are represented. As shown for the vortex valve, also for the double flow cyclone two different independent flows are incoming in a cylinder volume (1), one of the two flow is a supply, with a radial port in the vortex valve and axial in the double flow cyclone (2); in both cases there is a tangential flow (3) and an axial exit (4). In the vortex the tangential flow allows to regulate the supply; in the case of cyclone it allows to give a strong tangential component to the flow velocity. By this way it is possible to separate objects having different shape and size controlling independently the two inlet flows and taking advantage from the dynamic equilibrium of aerodynamics forces, weight and centrifugal force.

The basic model to describe the motion of a particle separated in a cyclone assumes the following assumption: to separate a particle it is necessary that the time of particle staying in cyclone must be equal or longer then the time to across the cyclone radially starting from the particle initial position to the cyclone wall.

The turn numbers completed by a turning particle, in the cyclone, is given by the following experimental expression [11]:

$$N_e = \left( L_c + \frac{Z_c}{2} \right) / H_c \quad (1)$$

In this expression  $L_c$ ,  $Z_c$ , and  $H_c$  are geometrical dimension, characteristic of the Cyclone.

Supposing equal the inlet velocity  $V_c$  of the gas and particle, the time of staying of the gas in the cyclone chamber is:

$$\Delta t = 2\pi r N_e / V_c \quad (2)$$

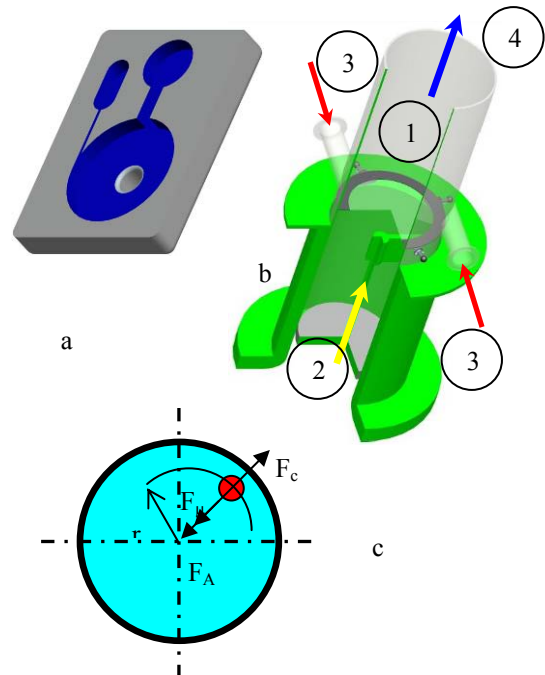


Figure 8 The multi flow cyclone and a vortex valve scheme.

This time is computed assuming the particle trajectory radius on a transversal plane respect to the cyclone axis, equal to the cyclone chamber.

Computing the radial particle velocity by two way: a cinematic ratio between the radial particle displacement and time and an equilibrium among centrifugal force, centripetal force due to the displaced flow and viscous force acting on the particle, it is possible to give the diameter  $D_p$  of the particle with  $\rho_p$  volumic mass, that can be separate for a given cyclone having  $B_c$  as radial dimension of inlet tangential port, an inlet flow with  $V_c$  velocity  $\mu$  dynamic viscosity,  $\rho$  gas volumic mass:

$$D_p = \sqrt{\frac{9\mu B_c}{\pi N_e V_c (\rho_p - \rho)}} \quad (3)$$



Figure 9 The multi flow cyclone

In Figure 9 the photograph represents the double flow cyclone. It is possible to see the cylindrical chamber, made by transparent material to allows optical measurements, the axial port with honeycomb grid, the tangential two ports and the axial superior exit. The cylindrical chamber is 0.90m height having a diameter of 0.80m and is supplied by two fans. The two fans powered by a 1kW motor for the axial flow and 2,0kW for tangential flow. The cyclone has two independent fans to supply the two different inlet ports. The tangential flow is generated by a centrifugal fan and the axial flow comes from an axial fan. To have two different flows generated independently allows to modulate the axial component of the flow velocity independently respect to the radial one. By this way it is possible to select the separation effect trying advantage from the equilibrium between weight and axial fluid dynamic forces and, on the other hand, the radial fluid dynamic effect and the centrifugal force.

The independent control of the axial and tangential flows allows to select the different object that will be separated.

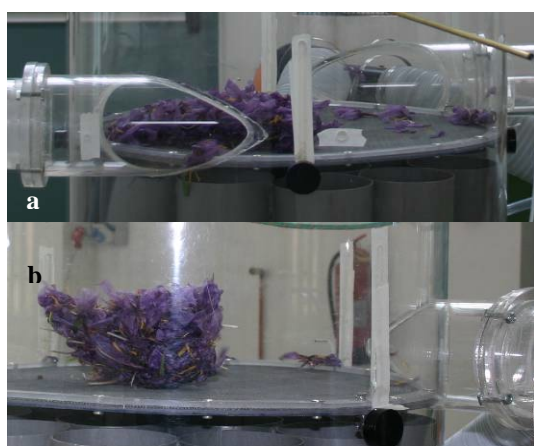


Figure 10 The incoming vortex with the Saffron flowers in the double flow cyclone cylindrical chamber

In Figure 10 two photographs show two different situations in the separation procedure: in Figure 10a the Saffron flowers are on the ground of the cyclone chamber, the flowers are distributed without any particular order; in Figure 10b the flowers are ordered at the centre of the chamber because of the tangential flow is activated.

The flowers and stigmas are collected around the chamber axis by the tangential flow, when is activated the axial one the flows composition performs the stigmas separation.

In Figure 11 an impact tube (Pitot configuration), to detect the total pressure of the flow, is shown. By this way it is possible to trace the velocity profile in the inlet zone of the tangential flow and to trace the speed field in the vortex cylindrical chamber.

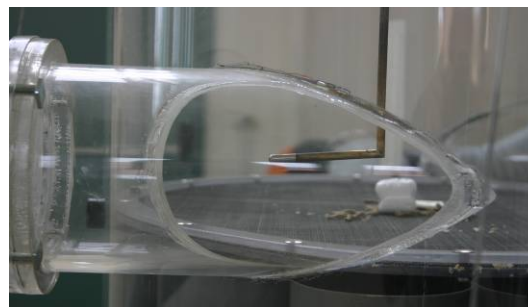


Figure 11 The total tube to detect the velocity profile near the tangential flow, incoming in the cylindrical chamber

A water gauge was employed to detect the pressure drop between total and static values of Pitot tube. The flow velocity profile at the inlet port of the tangential flow is traced in the graph of Figure 12. The graphs in this figure shows a turbulent flow situation, the Reynolds number is largely higher than  $1 \cdot 10^4$ , with a velocity distribution having an approximately constant medium velocity value in a region from the centre of the duct up to radius values near the chamber wall.

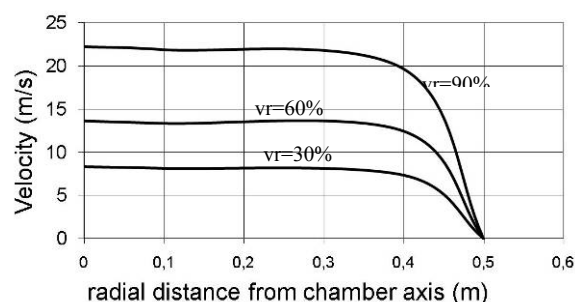


Figure 12 The flow velocity profile in one of the inlet ports for different fan velocities

The curves are given for different fan velocities ratio  $v_r$  corresponding to 30%, 60% and 90% of the maximum fan speed that is 3000 rpm.

The graphs in Figure 13 represent the flow velocity amplitude trend in the cylindrical chamber, detected by an impact tube, placed at a given height of 200mm, measured from chamber floor. The test conditions are referred to a flow generated by the only tangential flow, with the fan of the axial one stopped but leaving open the axial port. The curves are given for different fan velocities corresponding to 30%, 60% and 90% of the maximum fan speed that is 3000 rpm. The velocity trend is traced vs. the distance from the cylindrical chamber axis.

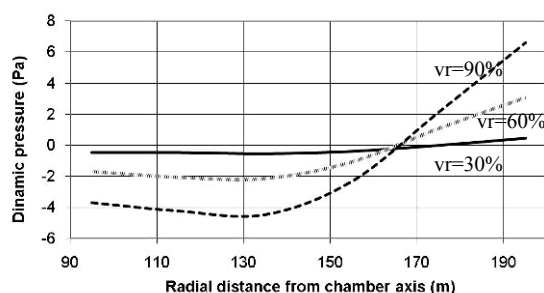


Figure 13 The flow velocity trend in the cylindrical chamber

It can be seen that the velocity amplitude is higher in a peripheral region, on the contrary the velocity is lower near the axis.

The total pressure values measured are quite low. The low pressure sensor used for the described tests are of the Gems family. The magnitudes calibrated and tested in factory instruments manufactures are referred in the table II

Table II - Low pressure transducer metrological parameters

Low pressure transducer	Range Pa	Accuracy	Supply voltage	Output
Gems Family	±50Pa	±1% FSa	10V	4-20 mA (0-10V)

#### 4 CONCLUSION

The prototypes illustrated in this paper demonstrates their efficiency in experimental tests performed both in laboratory and on field. Experimental tests performed are useful to individuate the working parameters to obtain a dynamic sufficiently fast to perform an efficient detaching and harvesting strategy and a velocity flow field to perform an efficient and rapid cleaning process of the spice.

#### 5 ACKNOWLEDGEMENTS

The research activity presented in this paper was financially supported by the Italian Ministry of Research (MIUR), by Sardegna Ricerche (Region of Sardinia - Italy) and Provincia del Medio Campidano in Sardinia.

#### REFERENCES

- [1] Ferraresi, C. and Manuello Bertetto, A. 1995., Self-adaptive three-fingered robot hand with tactile sensors, Proceedings of the fourth International Symposium of Measurement and Control in Robotics, pp. 275-280, Slovakia, June 12-16.
- [2] Ferraresi C., Manuello Bertetto A. and Mattiazzo G. 1995. A Low-Cost Pneumo-Electronic Tactile Sensor, ICRAM 95, Istanbul (Turkey), August 14-16, pp. 1098 – 1103.
- [3] M. Carello, M., Ferraresi, C., and Visconte, C. 2003. A new flexible pneumatic finger for a fruit-harvesting hand, 7th Int. Symp. On Fluid Control, Measurement and Visualization, Sorrento, (Italy), August 25-28.
- [4] Ruggiu, M. and Manuello Bertetto, A. 2006., A mechanical device for harvesting Crocus Sativus (Saffron) flowers, Applied Engineering in Agriculture, American Society of Agricultural and Biological Engineers(ASABE), Vol. 22 (4), pp 491-498.
- [5] Manuello Bertetto, A., Falchi C., Pinna R. and Ricciu R. 2010. An Integrated Device for Saffron Flowers Detaching and Harvesting, 19th International Workshop on Robotics in Alpe-Adria-Danube Region, Budapest (Hungary), 23-25 June.
- [6] Belforte G., Manuello Bertetto A., Mazza L. 1994. Analysis of Vortex Valves for Minimizing Control Flow, Proceedings of FLUCOME, Toulouse (France), pp.757-762.
- [7] Belforte G., Manuello Bertetto A., Mazza L. 1995. Effect of outlet diffuser and geometry optimisation of performance of vortex valves, 9th Congress on the Theory of Machines and Mechanisms IFToMM1995, Milano (Italy), pp.2611-2615.
- [8] Amol A. Kulkarni, Vivek V. Ranade, R. Rajeev R. and Koganti S. B. 2009. Pressure drop across vortex diodes: Experiments and design guidelines, Chemical Engineering Science, Vol. 64 (6), pp.1285-1292.
- [9] W. S. Lewellen W.S. 1971. A Review of Confined Vortex Flows, Report NASA CR 1772, July 1971.
- [10] Hill T. 2004. The Contemporary Encyclopedia of Herbs and Spices: Seasonings for the Global Kitchen, Wiley, ISBN 0-471-21423-X.
- [11] Wallace B. Smith, Rufus R. Wilson, Bruce Harris. 1979. A stage Cyclone system, Journal of American Chemical Society, Vol. 13 (11) pp.1387-1392.

# EVOLUTIONARY ALGORITHM TO SOLVE THE TRAJECTORY PLANNING PROBLEM, WITH ROBOT DYNAMICS CONSIDERATIONS

Fares J. Abu-Dakka

Francisco Valero

Jose Luis Suñer

Vicente Mata

Centro de Investigación de Tecnología de Vehículos, Universitat Politècnica de València - Valencia, Spain

## ABSTRACT

This paper presents a new genetic algorithm methodology to obtain a smooth trajectory planning for industrial robots in complex environments. This method aims to gradually create the collision free trajectory as the robot moves. The presented method deals with the uncertainties associated with the kinematic properties of intermediate via points since they are generated as the algorithm evolves towards the solution. As well as that, the objective of this algorithm is to minimize the trajectory time, which guide the robot motion. As an application example, this algorithm is applied over Puma 560 robot. Some numerical examples are provided in this paper to evaluate the functionality of the algorithm.

Keywords: trajectory planning, adjacent configurations, genetic algorithms, obstacles avoidance

## 1 INTRODUCTION

In the last few decades, the problem of minimum time trajectory planning for industrial robots has been addressed by numerous researchers motivated by the direct relation between executing tasks in the minimum amount of time and productivity.

The trajectory planning problem [1-8] has been analyzed a direct and indirect approaches. Indirect approaches firstly seek for a path in the configuration space, and then the trajectory adjusts, subject to the dynamic constraints of the manipulator [2]. On the other hand, the search takes place in the system's state space in the direct approaches [1, 5, 8]. The method used in this paper is oriented to avoid obtaining a prior path.

Numerous implementations of genetic algorithms (GAs) [9] in the field of robot trajectory planning have been developed in the last few decades. Toogood [10] developed a GA to find collision-free trajectories for the 3R robot with specific start and goal joint configurations, among known stationary obstacles. Moreover, free-obstacle trajectory planning is discussed [10].

For indirect approaches, the trajectories between via points are interpolated by means of cubic polynomial functions [1, 3]. Others used trigonometric splines, which ensure the continuity of the jerk [4]. Also, a quadratic jerk profile for a fifth degree polynomial spline is introduced [5].

By contrast, direct methods are presented in [11-13]. To obtain a practical trajectory, the manipulability measure can be used as decision criteria for robot trajectory planning [11]. A concatenation method of fifth-order polynomials with jerk limits has been studied [12]. A minimum-jerk 3D model used to obtain the desired path in Cartesian space [13].

In this paper, a mixed method is presented (in two stages) using GA for obtaining the minimum time trajectory for industrial robots (at least 6 Degree of Freedom) working in complex environments and in which the intermediate configurations are unknown. In the first stage, the algorithm optimizes the trajectory time depending on the optimized time from the Adjacent Configurations (AC); where the trajectory is composed of set of AC [14-16]. In the second one, the obtained trajectory time from the first stage is optimized using GA. This GA is subjected to continuous velocity and acceleration between intermediate configurations.

The algorithm works on a discretized configuration space which is generated gradually as the direct procedure solution evolves [2].

---

Contact authors: Fares Abu-Dakka<sup>1</sup>, Francisco Valero<sup>2</sup>

<sup>1</sup>Email: fares.abudakka@gmail.com

<sup>2</sup>Email: fvalero@mcm.upv.es

## 2 GENETIC ALGORITHM PROCEDURE

In this paper, three optimization processes using GAs are involved:

- (1) For the obtaining of the AC [14].
- (2) For the obtaining of the overall trajectory.
- (3) For the optimization of the time and make continuous connections for velocities and accelerations between via configurations.

The GA for AC uses the technique of steady-state (SSGA) reproduction without duplicates, creating a certain number of children to replace the parents, but discards duplicated children of current individuals in the population. The GA for trajectory uses parallel populations with migration. The GA has multiple independent populations. Each population evolves using SSGA, but at each generation some individuals migrate from one population to another. The migration algorithm is a deterministic stepping-stone. This means that each population migrates a fixed number of its best individuals to its neighbour. The master population is updated each generation with best the individual from each population.

## 3 ROBOT AND WORKSPACE MODELLING

The robot has been modeled as a wire linkage [16], see Figure 1. Furthermore, the robot configuration has been modelled as a function of joint variables  $C_j(q_i)$  [14]. Moreover, the robot configuration can be expressed in Cartesian coordinates as a set of points called significant points  $\alpha_{ij}(q_i)$  and interesting points  $P_{kj}(q_i)$  to facilitate the collision avoidance [14]. Significant points are dependent on the degrees of freedom of the robot. They should be as minimal in number as possible to define the robot without ambiguity. Interesting points are dependent on significant points.

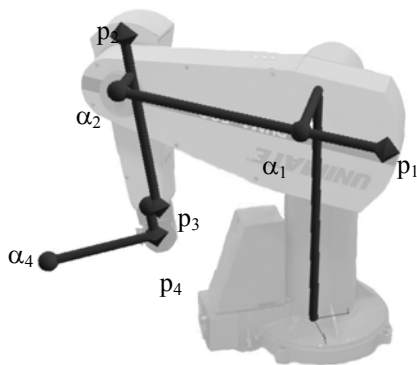


Figure 1 Robot wired model.

The workspace and obstacles are modelled in Cartesian coordinates. Obstacles are considered to be static and represented as a combination of three basic elements: Sphere, Cylinder, Prism [2, 14, 15]. The growing obstacles technique has been used [17].

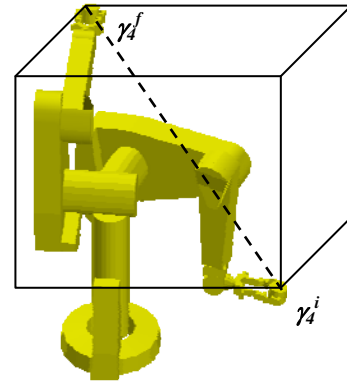


Figure 2 Workspace modelling.

## 4 OBTAINING AC WITH DYNAMIC COMPATIBILITY

The AC in this paper has been modelled and computed in the same manner published in [14]. The order in which the ACs are obtained will condition the Space of configurations generated and therefore, the whole trajectory [14-16].

Dynamic compatibility between the  $C_p$  and  $C_k$  must be presented. To verify this, a path is adjusted by means of interpolation polynomials, subjected to the robot's actuators limits. The problem of obtaining of the minimum time  $t_{pk}$  between the configurations is solved supposing zero velocities in the ends of the trajectory between the adjacent configurations.

The interpolation function has the form as in Eq. (1).

$$q_i^{pk} = a_i^{pk} + b_i^{pk} t_{pk} + c_i^{pk} t_{pk}^2 + d_i^{pk} t_{pk}^3 \quad (1)$$

In this paper, the inverse dynamic problem (IDP) was solved using the recursive Newton-Euler formulations [18].

## 5 OBTAINING THE TRAJECTORY

The determination of the trajectory from  $C_i$  is achieved in two stages:

- (1) Applying a random search algorithm to look for the next AC.
- (2) After the second AC, a continuous connection between every two adjacent cubic polynomials takes place until the end of the whole trajectory is reached.

Hence, a continuous trajectory is adjusted directly. It should be kept in mind that this time is still not optimal.

The objective is to minimize the travelling time  $t$ .

$$t = \sum_{i=1}^f t_{pk,i} \quad (2)$$

In each step of the evolution of the trajectory let us consider the trajectory fragment  $i-1$  (between  $C_k(q_k)$  and  $C_r(q_r)$ ) and fragment  $i$  (between  $C_r(q_r)$  and  $C_p(q_p)$ ) expressed in joint variables through the polynomials:

$$q^{rk}(t) = a^{rk} + b^{rk} t_{rk} + c^{rk} t_{rk}^2 + d^{rk} t_{rk}^3 \quad (3)$$

$$q^{pr}(t) = a^{pr} + b^{pr} t_{pr} + c^{pr} t_{pr}^2 + d^{pr} t_{pr}^3 \quad (4)$$

To guarantee the smoothness of the whole path, the following conditions are imposed:

(1) Position:

$$q^{rk}(0) = q_k \quad q^{pr}(0) = q_r \quad (5)$$

$$q^{rk}(t_{rk}) = q_r \quad q^{pr}(t_{pr}) = q_p$$

(2) Velocity:

$$\dot{q}^{rk}(0) = b^{rk}, \quad \dot{q}^{rk}(t_{rk}) = \dot{q}^{pr}(0), \quad \dot{q}^{fn}(t_{fn}) = 0 \quad (6)$$

(3) Acceleration:

$$\ddot{q}^{rk}(t_{rk}) = \ddot{q}^{pr}(0) \quad (7)$$

To validate the optimality, another GA procedure is fed by the trajectory obtained (from the previous stage). Its aim is to minimize that time using Clamped Cubic Spline.

Figures 1-4 show the kinematic and dynamic parameters corresponding to Row 0 in Table I. The torques limits in N.m. are:  $\tau_1, \tau_3 \in [-140, 140]$ ,  $\tau_2 \in [-180, 180]$ ,  $\tau_4, \tau_5 \in [-80, 80]$ ,  $\tau_6 \in [-40, 40]$ . (Blue = Joint 1, Pink = Joint 2, Green = Joint 3)

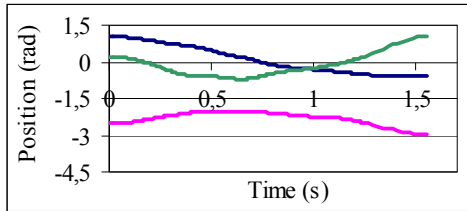


Figure 3 Joints position vs. execution time.

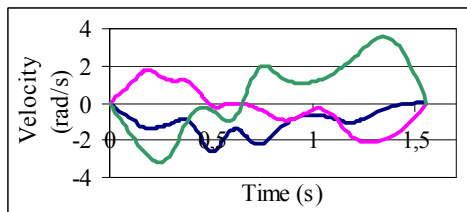


Figure 4 Joints velocities vs. execution time.

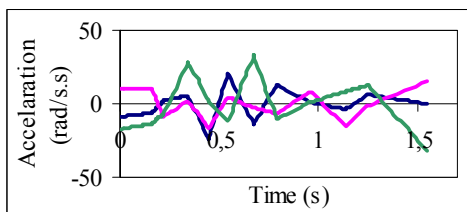


Figure 5 Joints accelerations vs. execution time.

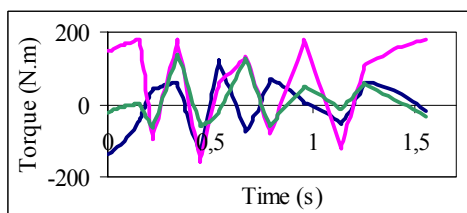


Figure 6 Joints torques vs. execution time.

## 6 GENETIC ALGORITHM OPERATORS

**Chromosome:** the chromosome is a complete trajectory between  $C_i$  and  $C_f$ . Each one is composed of a set of genes. Each gene contains two cells: (1) the first cell contains the robot configuration  $C\{q_1, q_2, \dots, q_i\}$ ,  $i = 6$  in case of the Puma 560 robot, and (2) the second cell represents the time needed to move the robot from the previous configuration to this configuration saved in the gene.

$$Chromosome = \left\{ \begin{array}{l} [C^0(q_j), T=0], \dots, \\ [C^n(q_j), T=t_n], \dots, \\ [C^f(q_j), T=t_f] \end{array} \right\} \quad (8)$$

The first gene contains the  $C_i$  data. Then the ramification starts to construct the trajectory by randomly selecting the next gene; based on the random search algorithm; by calling the AC builder algorithm, and so on to the final configuration. The ramification occurs without repetition in the  $X, Y, Z, XY, XZ, YZ$ , and  $XYZ$  directions. In this paper, chromosomes may have unequal lengths.

**Objective function:** the objective is to minimize Eq. (2).

**Crossover:** the crossover occurs when its probability is satisfied. The crossover is made through the exchange between two selected trajectories. In the selected parents, the algorithm searches the genes of each trajectory for the intersection configurations. The intersection in this case is to find a  $(C_{jp})$  configuration  $p$  in trajectory  $i$  that can be adjacent to a  $(C_{jk})$  configuration  $k$  in the trajectory  $j$ . The algorithm looks for all possible intersections between two selected trajectories for crossover. i.e. given two trajectories: *Dad* with length  $n$  and *Mom* with length  $m$ .

$$Dad = C_{Dad}^1 \cup C_{Dad}^2 \cup \dots \cup C_{Dad}^i \cup \dots \cup C_{Dad}^n \quad (9)$$

$$Mom = C_{Mom}^1 \cup C_{Mom}^2 \cup \dots \cup C_{Mom}^j \cup \dots \cup C_{Mom}^m \quad (10)$$

$$Dad \cap Mom = \left\{ (C_{Dad}^k, C_{Mom}^p), \dots, (C_{Dad}^l, C_{Mom}^p) \right\} \quad (11)$$

where  $l = 0, 1, 2, \dots, n-2$  in case of *Dad* or  $m-2$  in case of *Mom* number of AC found.

One intersection will be randomly selected in case many are found satisfying these criteria. Hence, the new offspring (trajectory) will be like this:

$$Offspring = C_{Dad}^1 \cup C_{Dad}^2 \cup \dots \cup C_{Dad}^i \cup C_{Mom}^j \cup \dots \cup C_{Mom}^m \quad (12)$$

If there is no intersection, the crossover will be cancelled. The resulting trajectory will consist of a part from *Dad* (from the initial configuration until the selected  $C_i$ ), and a part from *Mom* (from  $C_j$  until the final configuration). This method of crossover does not need equal chromosomes lengths.

**Mutation:** mutation is done by selecting a gene randomly from a selected trajectory. The first and the final configurations are not considered for mutation. The configuration is then compared to the previous and next configurations in the trajectory. All possible changes with

which the trajectory will remain incremental and quantum are applied to the configuration. For illustration, let us consider three consecutive robot configurations  $C_{i-1}$ ,  $C_i$ ,  $C_{i+1}$  in which their end-effector have the positions  $(0, 0, 0)$ ,  $(1, 0, 1)$ ,  $(1, 1, 2)$  with a step value of 1 in the  $x$ ,  $y$  and  $z$ -coordinates. If mutation is to be applied on the  $C_i$ , where its end-effector position lies at  $(1, 0, 1)$ , the algorithm will consider how each of the coordinates changed. The  $x$ -coordinate changed from 0 (previous position) to 1 and remained 1 in the next position. It is clear that this change will not affect the validity of the trajectory since the positions will become  $(0, 0, 0)$ ,  $(0, 0, 1)$ ,  $(1, 1, 2)$ ; i.e. the  $x$ -coordinate changed from current position to next, while remained the same when going from the previous position to the current one. The same thing can be said about the  $y$ -coordinate, since it has not changed when going from the previous position to the current one, while it has changed when going to the next position. The mutation will cause the  $y$ -coordinate to change from 0 to 1. Finally, the  $z$ -coordinate can't be modified since it changed from 0 to 1 to 2. If the mutation would change the  $z$ -coordinate to 0 or 2, the step would be greater than the predefined step. The mutation will not affect the coordinates that have not changed at all, for example the  $x$ -coordinate in  $(0, 0, 0)$ ,  $(0, 0, 1)$ ,  $(0, 1, 1)$  since any changes will result invalid trajectory. For this new position, the AC algorithm will move the robot from the position  $(0, 0, 0)$  to  $(0, 0, 1)$  and then to  $(1, 1, 2)$ .

## 7 APPLICATION EXAMPLES

The algorithm has been tested using the Puma 560 robot on an Intel Xeon CPU E5440 @ 2.83 GHz, 8 GB of RAM. Three operational parameters have been studied to evaluate the efficiency of the presented procedure:

- (1) Execution Time ( $t_e$ ).
- (2) Travelled distance by significant points ( $d_s$ ).

$$\sum_{j=1}^4 \sqrt{(\alpha_j^k - \alpha_j^p)_x^2 + (\alpha_j^k - \alpha_j^p)_y^2 + (\alpha_j^k - \alpha_j^p)_z^2} \quad (13)$$

- (3) Computational time ( $t_c$ ).

**Example 1:** This example has been solved in [11] where a harmonic function was used for interpolation.

Figure 7 shows the robot initial and final configurations for the case of three obstacles.

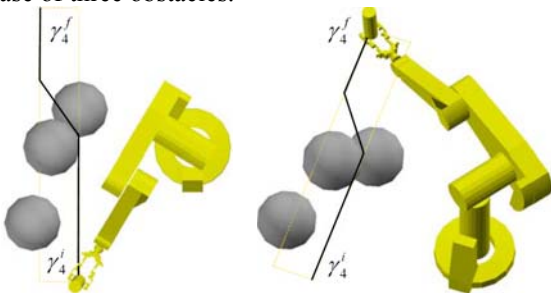


Figure 7 Example 1.

Table I - Example 1 results.

	Operational parameters	Results of this paper	Results [11]		
			A *	UC	greedy
0	$t_e$ (s)	1.552	22.15	21.67	26.16
	$d_s$ (m)	3.9446	3.65	3.65	4.19
	$t_c$ (s)	4876	2691.27	2785.20	555.55
1	$t_e$ (s)	1.80759	21.63	27.61	49.98
	$d_s$ (m)	4.0642	4.48	4.11	5.94
	$t_c$ (s)	7321	2360.28	2182.93	294.74
2	$t_e$ (s)	1.96055		32.48	46.32
	$d_s$ (m)	4.1335		5.81	5.71
	$t_c$ (s)	6749		735.32	70.30
3	$t_e$ (s)	2.67079	22.30	28.97	38.21
	$d_s$ (m)	4.2554	5.35	4.90	5.57
	$t_c$ (s)	6799	257.58	371.74	88.40

Moreover, [11] solved 20 examples in his article obtained in base of 5 different combinations of initial and final configurations of the robot. Each combination has been solved in 4 different workspaces. These examples are resolved using the presented GA procedure.

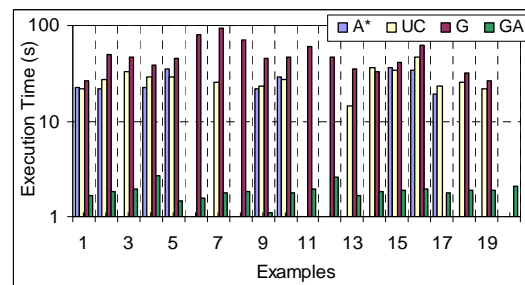


Figure 8 Execution time comparison between GA and [11] procedure.

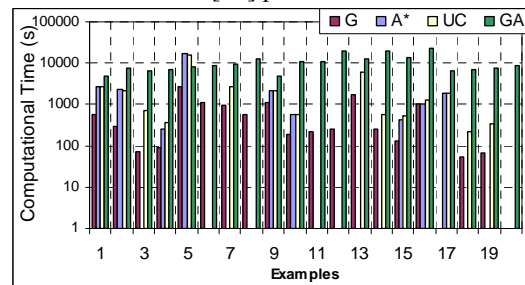


Figure 9 Distance comparison between GA and [11] procedure.

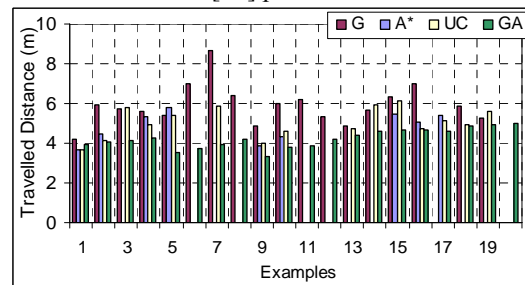


Figure 10 Computational time comparison between GA and [11] procedure.

Observing the results of the 20 examples, it could be seen clearly that the execution time obtained by the GA procedure present an improvement comparing it with the results published in [11] by an average 43%. Moreover, the travelled distance by significant points in the most of cases present an improvement in comparison with results from [11].

**Example 2:** This example demonstrates the ability to adapt the algorithm in absence or presence of obstacles.

Table II - Example 2 results.

	$t_e$ (s)	$t_c$ (s)	$d_e$ (m)	$d_s$ (m)
0 Obs	2.42217	12915	1.7106	4.7870
With Obs.	3.85854	57080	1.7802	5.2227

The next Figure 11 shows the robot in the initial and final configuration, the end-effector track, and the workspace.

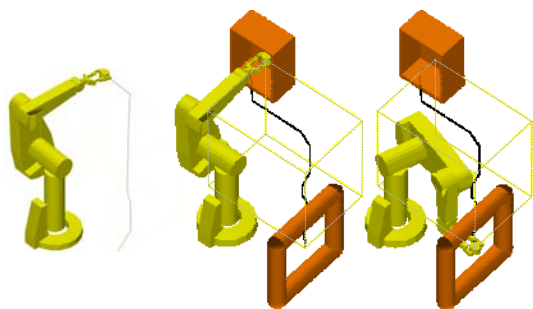


Figure 11 Example 2 (Case with and without obstacles).

## CONCLUSION

In this paper, a GA approach has been introduced to solve the trajectory planning problem for industrial robots operating in complex 3D environments. The algorithm aims to minimize the time needed to move the robot from a  $C_i$  to a  $C_f$  avoiding the collision with the obstacles.

The presented algorithms have been tested using the above illustrated examples. The first example was composed of 20 different workspaces and the second one composed of 2 workspaces. The analysis of the results shed light on the characteristics and properties of the algorithms used. Part of these examples is compared with the work of other authors and demonstrates the efficiency of the proposed procedure by an average of 43%. The other part of the examples used “close to real” industrial scenario to show the ability of the algorithm to adapt to any workspace.

As shown in the examples, computational time is high. Moreover, it increases as the restrictions increase. The number of individuals should be increased and so on the number of generations for more accurate results using the GA procedure, especially for big problems, which leads to higher computational time. This may consider as a disadvantage of the GA in general. However, as the industrial robots do repetitive trajectories, an offline planning normally takes place. This means that the

computational time cost can be acceptable as the resulting planning and time trajectory are good enough.

## ACKNOWLEDGMENT

This paper has been possible thanks to the funding of Spanish Education, Culture and Sport Ministry by means of the Researching and Technologic Development Project IDEMOV DPI2010-20814-C02-01.

## REFERENCES

- [1] S. F. Saramago and V. Steffen, Trajectory modeling of robot manipulators in the presence of obstacles. *Journal of optimization theory and applications*, Vol. 110, No. 1, pp. 17-34, 2001.
- [2] F. J. Valero, V. Mata, and A. Besa, Trajectory planning in workspaces with obstacles taking into account the dynamic robot behavior. *Mechanism and Machine Theory*, Vol. 41, pp. 525-536, 2006.
- [3] A. Piazzzi and A. Visioli, A Global Optimization Approach To Trajectory Planning For Industrial Robots. *Proc. of IEEE-RSJ Int. Conf. on Intelligent Robots and Systems*, pp. 1553-1559, 1997.
- [4] A. Piazzzi and A. Visioli, Global minimum-jerk trajectory planning of robot manipulators. *IEEE Transactions on Industrial Electronics*, Vol. 47, No. 1, pp. 140-149, 2000.
- [5] A. Gasparetto and V. Zanotto, A new method for smooth trajectory planning of robot manipulators. *Mechanism and Machine Theory*, pp. 455-471, 2007.
- [6] E. Bertolazzi, F. Biral, and M. D. L. M, Real-time motion planning for multibody systems - Real life application examples. *Multibody System Dynamics* Vol. 17, No. 2-3, pp. 119-139, 2007.
- [7] S. Behzadipour and A. Khajepour, Time-optimal trajectory planning in cable-based manipulators. *IEEE Transactions on Robotics*, Vol. 22, No. 3, pp. 559-563, 2006.
- [8] L. d. Plessis and J. Snyman, Trajectory-planning through interpolation by overlapping cubic arcs and cubic splines. *International Journal for Numerical Methods in Engineering*, Vol. 57, No. 11, pp. 1615-1641, 2003.
- [9] J. H. Holland, *Genetic Algorithms*. Scientific American, pp. 66-72, 1992.
- [10] R. Toogood, H. Hao, and C. Wong, Robot path planning using genetic algorithms. *Proc. of IEEE International Conference on Systems, Man and Cybernetics*, Vancouver, BC, Canada, pp. 489-494, 1995.
- [11] F. J. Rubio, F. J. Valero, J. L. Suñer, and V. Mata, Simultaneous Algorithm to Solve the Trajectory Planning Problem. *Mechanism and Machine Theory*, Vol. 44, pp. 1910-1822, 2009.

- [12] S. Macfarlane and E. Croft, Jerk-bounded manipulator trajectory planning: Design for real-time applications. *IEEE Transactions on Robotics and Automation*, Vol. 19, No. 1, pp. 42-52, 2003.
- [13] K. Abdel-Malek, J. Y. Z. Mi, and K. Nebel, Optimization-based trajectory planning of the human upper body. *Robotica*, Vol. 24, pp. 683-696 part 6, 2006.
- [14] F. Abu-Dakka, F. J. Valero, and V. Mata, Obtaining Adjacent Configurations with Minimum Time Considering Robot Dynamics Using Genetic Algorithm. *Proc. of 17th International Workshop on Robotics in Alpe-Adria-Danube Region*, Ancona, Italy, 2008.
- [15] F. Abu-Dakka, F. J. Valero, A. Tubaileh, and F. Rubio, Obtaining Adjacent Configurations with Minimum Time Considering Robot Dynamics. *Proc. of The 12th World Congress in Mechanism and Machine Science*, Besançon, France, 2007.
- [16] F. J. Valero, V. Mata, J. I. Cuadrado, and M. Ceccarelli, A formulation for path planning of manipulators in complex environments by using adjacent configurations. *Advanced Robotics*, Vol. 11, pp. 33-56, 1997.
- [17] T. Lozano-Pérez and M. A. Wesley, An Algorithm for Planning Collision-Free Paths Among Polyhedral Obstacles. *Communications of ACM*, Vol. 22, pp. 560-570, 1979.
- [18] J. J. Craig, *Introduction to Robotics Mechanics and Control*. 2 ed. Addison-Wesley Publishing Company, 1989.

# FAST RANGE IMAGE SEGMENTATION FOR A DOMESTIC SERVICE ROBOT

Peter Einramhof

Robert Schwarz

Markus Vincze

Vienna University of Technology, Automation and Control Institute

## ABSTRACT

In this paper we present a fast approach to range image segmentation. The segmentation results are intended to serve as input to the perception system of a domestic service robot, which requires real-time capability due to the robot's interaction with a dynamic environment. In the first step mixed pixels at depth discontinuities are identified. This is followed by extracting step and roof edges. Planar patches are detected with a focus on horizontal and vertical planar structures due to their dominance in manmade environments and importance in robotic tasks. Finally, the range data is labelled with the locally dominant features, which results in a label map. Our approach was tested on real range images recorded in a home-like office environment using a tilting laser range finder.

Keywords: range images, segmentation, service robotics, tilting laser range finder

## 1 INTRODUCTION

In "classic" service robotics the focus lies on transporting objects in well-structured and controlled environments like factories, hospitals or offices. In such environments a simple perception system is sufficient to provide data for the necessary tasks of the robot, namely self localisation and obstacle avoidance. The most popular sensor is a 2D laser range finder scanning parallel to the ground. The environment is modelled in a 2D fashion (2D grid or feature maps) since the presence of many unobstructed vertical structures such as walls or the faces of file drawers and closets allow for this approach. Processing the sensor data, for instance 361 range measurements for one 180° scan of the laser range finder, requires only very little computational power to work in real-time, which is a necessity since the robot is moving in a dynamic environment.

In domestic service robotics the demands to the perception system are higher in comparison. Home environments are challenging since they are cluttered and less structured. There are amorphous surfaces like curtains or other home textiles, and protruding surfaces such as table tops.

The three-dimensional nature of this environment can no longer be neglected. To be useful for the in general

technically non-trained users, the offered services must be more than just safely navigating from A to B. The perception system has to support grasping and object detection, for instance. The latter also contributes to more natural human-robot interaction since it is closer to human perception – the user would rather like to call the robot to "the sofa in the living room" than to  $(x, y, \theta)$ .

When changing over from 2D to 3D data (more exactly: 2.5D data), the demands to the computational part of the perception system rise drastically due to the increased amount and complexity of the data. Nevertheless, the real-time requirement still stands. Since mobile robots run on batteries and a long time of autonomy is desired, the onboard computational power cannot be increased arbitrarily (not to mention cost, size, heat and noise generation). To achieve real-time responsiveness despite this restriction, fast segmentation algorithms are required.

In this work we address range image segmentation under real-time constraints as well as detection and removal of mixed pixels, outliers that occur at discontinuities within the range image. The features extracted in the course of our segmentation approach are intended to be useful for various tasks of indoor service robotics: horizontal planar structures provide information for safe navigation and about support planes, vertical planar structures can be used for map building and self localisation, and finally, step and roof edges define object boundaries and the transition between objects and support plane or between object parts.

---

Contact author: Peter Einramhof<sup>1</sup>

<sup>1</sup>Gusshausstrasse 27-29, 1040 Vienna, Austria.

The remainder of this paper is structured as follows: Section 2 gives an overview of related work. Section 3 provides the motivation for the features we have selected as target result and describes our approach in detail. Section 4 provides experimental results on data recorded with a tilting laser range finder. Finally, Section 5 concludes with a summary and an outlook.

## 2 RELATED WORK

When compared to intensity or colour images, which provide information about the surface properties of the objects observed by a sensor, range images encode the three-dimensional structure of the observed scene.

The purpose of range image segmentation is to divide the image into features or regions that are meaningful with respect to a given task. Despite a history of about three decades, there still is no standard approach to range image segmentation. Depending on the task, constraints, assumptions made about the nature of the content of the range image, and whether specific properties of the sensor are incorporated, algorithms range from fast ad hoc solutions to slow(er) sophisticated methods.

Comparison of quality and performance of different segmentation methods is difficult due to the lack of sound experimental evaluation. An exception is the field dealing specifically with the segmentation of objects with planar faces, published by Hoover et al. together with experimental data [8]. A detailed overview of literature in that field is provided by Haindl and Zid [4]. Segmentation methods can be roughly divided into edge-based and region-based approaches.

Edge-based methods are inspired by human vision since humans have the principle that there is an edge or discontinuity of some kind between two separable objects [11][16]. Edge pixels have a gradient assigned, that is, magnitude and direction of the greatest local change. Sappa and Devy use an edge-based segmentation technique that consists of two stages: the first stage generates a binary edge map based on scan line approximation that considers only two orthogonal scan line direction. The second stage links the edge points by applying a graph strategy [12]. Bellon and Silva present range image segmentation based on edge detection techniques with the aim of better preserving the object topology and shape in noisy range images. Their approach avoids fixed thresholds for being useful in unsupervised systems [1]. Han et al. propose a jump-diffusion method for segmenting a range image and its associated reflectance image in a Bayesian framework [5]. Harati et al. propose the metric “bearing angle”, which the incidence angle between the measurement beam and a surface. By thresholding the bearing angle and its first derivative, step and roof edges are detected. Since their target application is 3D indoor SLAM they are rather interested in the remaining planar patches and thus remove all edges [6].

Region-based methods group pixels into regions using the criteria of proximity and homogeneity. These methods achieve grouping either by splitting the image into smaller regions [10], merging small regions into larger ones [8], or splitting and merging until all criteria are maximally satisfied [2][7][9]. In more recent work Gotardo et al. present a robust estimator, derived from the RANSAC and MSAC estimators, whose optimization process is accelerated by a genetic algorithm. Their range image segmentation algorithm is based on planar surface extraction in preserving small regions and edge locations when processing noisy images [3]. Similarly, Wang and Suter propose a highly robust estimator (Maximum Density Power Estimator), which applies nonparametric density estimation and density gradient estimation techniques in parametric estimation (“model fitting”). According to the authors it can tolerate more than 85% outliers [14]. Weingarten et al. use probabilistic plane fitting to extract large planar surfaces from range images as input to mapping the environment for mobile robotics [15]. Similarly to Bellon and Silva [1], we also make use of standard image processing as much as possible for edge detection. To increase robustness, various methods are combined in a voting scheme, and also the metric “bearing angle” [6] is incorporated.

## 3 APPROACH

In this section we discuss what features are extracted in the course of our segmentation approach as well as their relevance in the context of domestic service robotics. This is followed by a detailed discussion of the individual processing steps of our approach.

### 3.1 TARGET FEATURES

In (manmade) indoor environments horizontal and vertical planar structures are dominant; together they also define the room structure.

Horizontal planar structures such as the ground, table tops or the seats of chairs play the role of support planes on which the robot moves and on which obstacles or objects of interest are located.

Vertical planar structures are from walls, the faces of closets or the bodies of objects. Especially walls define the boundaries of the indoor environment and can serve as features for the robot’s self localisation.

In order to give meaning to the terms “horizontal” and “vertical”, a reference is required. This reference is the direction of gravity, to which vertical (horizontal) structures are parallel (perpendicular). This reference information is incorporated into the sensor data and the associated processing algorithms via the known geometry and kinematics of the setup consisting of sensor and robot, and optionally via inclinometers to take dynamic pitch and roll angles due to the robot’s motion into account.

Step edges occur at object boundaries, more exactly at the transition between foreground and background. We consider step edges as part of foreground objects.

Roof edges occur at the transition between parts of objects or between object and support plane, and also at top rims and high-curvature surfaces. Roof edges can be concave or convex.

### 3.2 MIXED PIXELS

In range images (or equivalently: depth images) from tilting laser scanners, time-of-flight cameras and also stereovision, there are range measurements at depth discontinuities that do not correspond to any physical structure. These mixed pixels have values that lie somewhere between the valid foreground and background range measurements (Figure 1). They are problematic because they seemingly connect foreground and background points to one contiguous object and thus have to be removed.

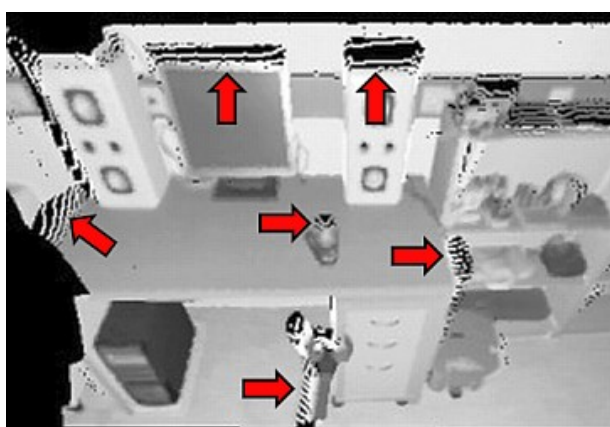


Figure 1 3D data of a gripper approaching a table scene. At depth discontinuities mixed pixels occur (marked by arrows).

The first step in detecting mixed pixels is to find depth discontinuities, that is, abrupt changes in the values of neighbouring pixels of the range image. But what extent of change is “abrupt”? Clearly, this depends on the measurement noise of the used sensor. To determine the noise level, we compute the standard deviation of the range values for each pixel within a 3x3 neighbourhood. Figure 2, right, shows that the standard deviation is high at depth discontinuities – in fact, the result is qualitatively equivalent to the gradient magnitude produced by a Sobel filter.

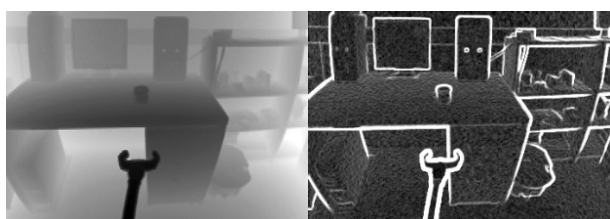


Figure 2 *Left*: range image. *Right*: standard deviation for each pixel of the range image within a 3x3 neighbourhood. Maximum deviation was clipped to 0.05m for better visibility of low deviation regions.

The standard deviation computed for each pixel votes for a bin of a histogram with a bin width of 1mm. We determine the location of the (first) peak of the histogram and consider it as “sigma” of the noise. Three times this “sigma” serves as threshold to determine depth discontinuities within the standard deviation image. While this threshold works well, there is a problem when neighbouring pixels’ beams intersect with planar structures at larger distances and at a flat angle (Figure 3, left). In such cases the local change in measured range is well above the threshold and would thus register as discontinuity.

In [6] Harati et al. propose the metric “bearing angle” (Figure 3, right), which is the incidence angle between the measurement beam and a surface. At real depth discontinuities this angle ( $\beta_i$ ), Equations (1) and (2), takes values close to  $0^\circ$  or  $180^\circ$ , i.e. the beam is close to parallel to the surface.

$$d_i = \sqrt{r_i^2 + r_{i+1}^2 - 2r_i r_{i+1} \cos \Phi_i} \quad (1)$$

$$\beta_i = \arccos\left(\frac{r_i - r_{i+1} \cos \Phi_i}{d_i}\right) \quad (2)$$

Although Harati et al. use solely this metric, it is problematic at short range i.e. objects close to the sensor, like in the case of a table scene. Due to the in general small angular increment  $\Phi_i$  between two neighbouring measurement beams,  $r_i$  and  $r_{i+1}$ , and the resulting small lateral distance between them at close range, the bearing angle  $\beta_i$  rather reflects the measurement noise than the geometry of the scanned object in such cases.

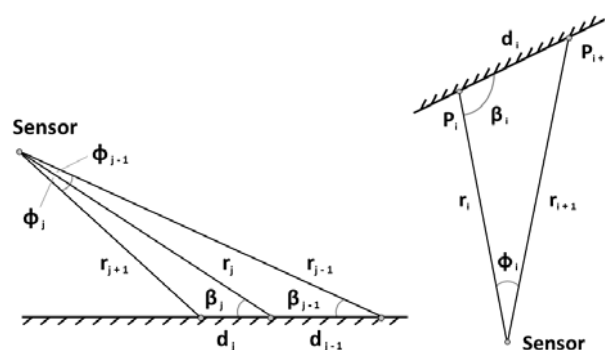


Figure 3 *Left*: three neighbouring range measurement  $r_{j-1}$ ,  $r_j$  and  $r_{j+1}$  of a column of the range image that intersect with a horizontal plane, e.g. the ground at a flat angle (viewed from the side). *Right*: horizontal bearing angle  $\beta_i$  (viewed from above).  $r_i$  and  $r_{i+1}$  are two neighbouring range measurements of a row of the range image, enclosing an angular increment  $\Phi_i$ .  $d_i$  is the distance between the intersection points  $P_i$  and  $P_{i+1}$  of the measurement beams  $r_i$  and  $r_{i+1}$  with the surface.

Since thresholding the standard deviation image yields wrong depth discontinuities at greater distances and thresholding the bearing angle yields wrong depth discontinuities at close distances, we multiply both thresholding results, which leave only discontinuities where both methods agree (Figure 4, top left). The threshold value for the bearing angle depends on the sensor; for our setup we experimentally found angles of smaller or equal  $5^\circ$  or greater or equal  $175^\circ$ , respectively, indicating discontinuities.

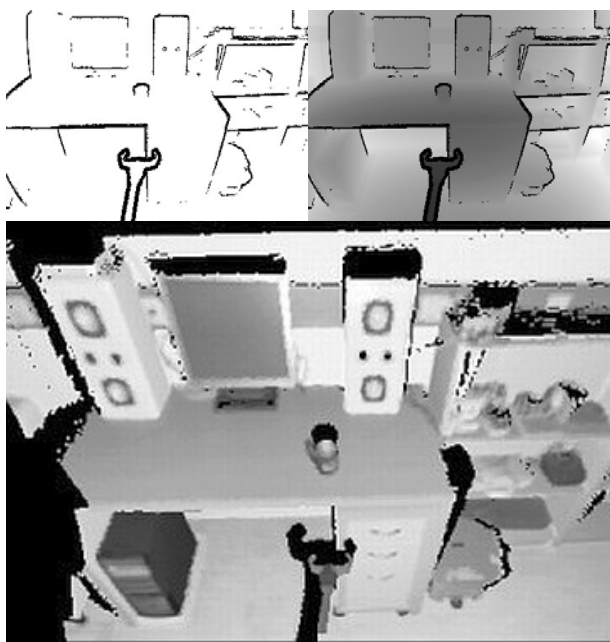


Figure 4 Top left: mask for mixed pixels removal. Top right: mixed pixels removed from range image. Bottom: 3D data computed from masked range image.

### 3.3 STEP EDGES

In our definition step edges are pixels of the range image at depth discontinuities that (1) are valid pixels and (2) belong to the foreground. Thus, they represent boundaries of foreground objects.

We first smooth the range image using a  $7 \times 7$  Gauss filter ( $\sigma = 1.0$ ). The previously computed mixed pixel mask (Figure 4, top left) defines “no-go areas” so as not to smooth over depth discontinuities. In the next step, the filtered range image is convoluted with a  $3 \times 3$  mask that has “-8” as central element and ones as 8-neighbours (Laplace filter). The result is an image that has positive values at the edges of foreground objects (Figure 5, left). At smooth parts of the range image, there is only a small response due to noise. Negative values are replaced by zero and a histogram of the positive values is created. Like described in the previous section, the location of the first peak is detected and three times its value is used as threshold. Finally, single-standing pixels that have no further pixel in its 8-neighbourhood are removed since they stem from noise (Figure 5, right).

### 3.4 ROOF EDGES

Step edges are added to the mask containing the mixed pixels. Again, this mask defines no-go areas for a second smoothing step. A  $3 \times 3$  median filter is applied to the previously Gauss-filtered range image.

From the smoothed range image, the horizontal and vertical bearing angles are computed. Furthermore, the bearing angles at each pixel are adjusted by the horizontal and vertical deflection angle of the measurement beam so that pixels belonging to planar structures have constant values of the bearing angles (Figure 6, top row). As suggested by Harati et al. [6], each bearing angle image is subjected to edge detection; we use a horizontal  $3 \times 3$  Sobel mask on the horizontal and a vertical Sobel mask on the vertical bearing angle image. The resulting two edge images are thresholded. We use  $15^\circ$  as minimum local change of the bearing angle. The roof edges from the thresholding results for the horizontal and vertical bearing angle are combined (Figure 6, bottom left).

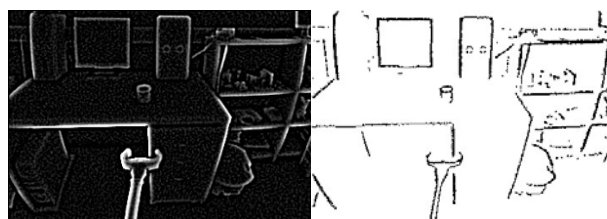


Figure 5 Left: result of Gauss-filtering the range image and subsequently convoluting it with a  $3 \times 3$  Laplace mask. Right: step edges after thresholding the Gauss- and Laplace-filtered range image.

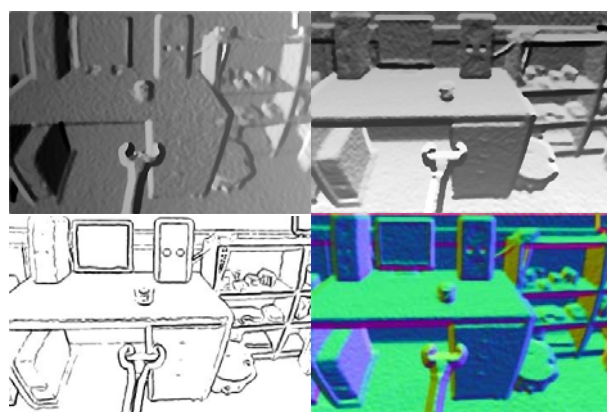


Figure 6 Top: horizontal and vertical bearing angle. Bottom left: roof edges. Bottom right: surface normals.

### 3.5 HORIZONTAL & VERTICAL PLANAR PATCHES

From the same smoothed range image as the bearing angles were computed, we also calculate the surface normals (Figure 6, bottom right). First, we compute 3D points from the valid points of range image. The coordinates of each 3D point are stored in individual arrays of the same size as the initial range image and at the same array cell position as its

associated range value. In this way the initial neighbourhood is maintained. For 3x3 pixel patches in regions without mixed pixels or step and roof edges two vectors are computed from the left- and rightmost and the top- and bottom-most 3D point in that patch. Finally, by applying the cross product to both vectors and by normalizing the resulting vector's length, we get the surface normal.

The surface normals are multiplied (dot product) with the unit vector of the vertical axis. As stated earlier, the information about the vertical direction has to be supplied from outside, either from the known geometry of the setup or from inclination sensors. The result of the dot product is thresholded. We allow a deviation of  $10^\circ$  from the vertical axis (horizontal plane) for the surface normals of horizontal (vertical) planar structures.

### 3.6 LABEL MAP

Mixed pixels, step edges, roof edges, vertical and horizontal planar patches have so far been stored in individual maps that have the same size as the initial range image from which they were derived. To each pixel of the range image we assign a label according to the locally dominant feature type. If more than one feature type has activation at a pixel location, a prioritization is applied: Mixed pixels, then step edges, roof edges, vertical and finally horizontal planar patches. The result is a label map (Figure 8, right column).

## 4 RESULTS

The following two subsections describe the sensor used for data acquisition and the data itself as well as practical results achieved on that test data.

### 4.1 TEST DATA

A tilting 2D laser range finder (Figure 7) built from a SICK LMS 100-10000 scanner and a SCHUNK PW 70 rotary tilt unit was used to capture test data. Each captured frame provides 360x500 range and intensity measurements. With an angular resolution of  $0.25^\circ$  horizontally and  $0.125^\circ$  vertically, the field of view is  $90^\circ(H) \times 62.5^\circ(V)$ .

The sensor was mounted onto a mobile robot at a height of about 125cm with respect to the ground. The top of the vertical field of view is parallel to the ground plane, its bottom is tilted downwards by  $62.5^\circ$ . This configuration allows scanning table scenes as well as detecting obstacle directly in front of the robot and up to the robot's height.

One 3D scan takes about 20 seconds. In order to simulate a frame rate of about 11Hz, a stop-motion technique was applied. That is, after each scan the robot and dynamic objects in the scene were moved by a small distance or angle according to the simulated speed and frame rate.

The data consists of 14 sequences with a total of 2,136 frames. Sequences addressing the tasks of obstacle detection and self localisation were recorded while the mobile robot was moving through several rooms of the test environment (e.g. Figure 8 mid and bottom, Figure 9 left

column). Sequences addressing object detection and grasping feature scenes with objects on tables and counters as well as a robotic gripper in action (e.g. Figure 4, Figure 8 top, Figure 9 top right).



Figure 7 Tilting laser range scanner for capturing the test data.

### 4.2 EXPERIMENTAL RESULTS

Our approach was implemented in C++ and tested on an Intel Core i5-430M notebook (2.24GHz, 4GB RAM) running 32bit OpenSUSE Linux 11.2. No optimizations such as SSE or multi-threading have been incorporating yet. The total amount of memory allocated for various buffers and lookup tables is slightly less than 3MB.

The segmentation processing chain was applied to the recorded sequences at four different resolutions. Table I provides the respective average processing times per frame. It shows that computational complexity of our approach is linear with respect to the number of pixels of the input range images.

Table I - Computation times at different resolutions

Resolution	Pixel count	Time (ms)
360x500	180,000	45.4
<b>360x250</b>	<b>90,000</b>	<b>22.3</b>
250x160 (bilinear)	40,000	10.8
180x125	22,500	5.7

Figure 8 shows range images and associated label maps for three tasks a domestic service robots might have: grasping a cup on a table (top row), opening or closing a door (mid row), and detecting the closest obstacles within a relevant height region for obstacle avoidance (bottom row). Figure 9 shows applications of the extracted features in the context of service robotics.

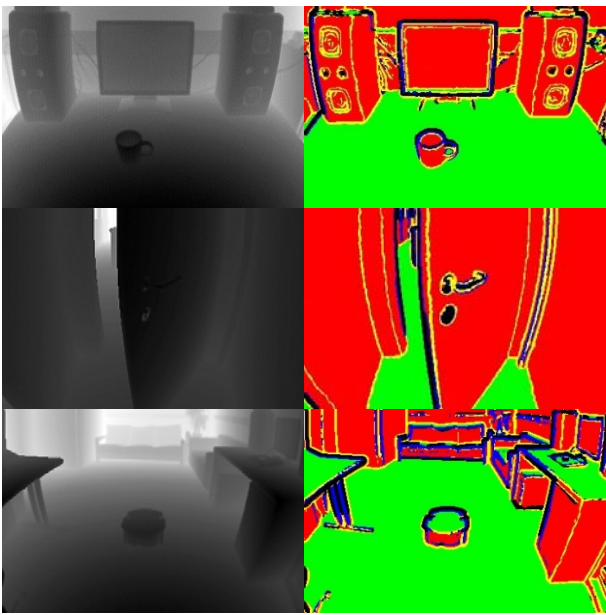


Figure 8 Range images (left column) and associated label maps for three scenes: objects on a table (top row), door handle (middle row), obstacles on the ground (bottom row). In each label map mixed pixels are black, step and roof edges are blue and yellow, and horizontal and vertical structures are green and red.

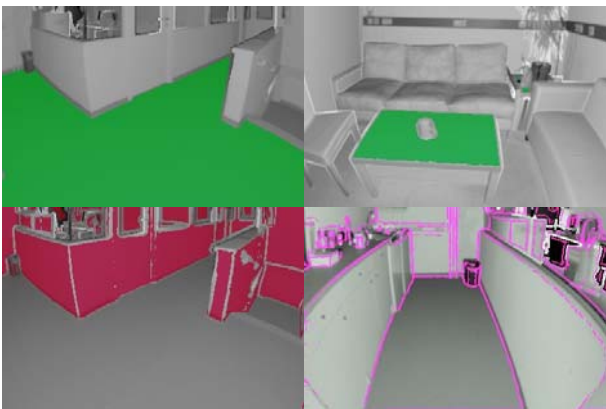


Figure 9 Examples for applications of the extracted features. Horizontal planar patches for obstacle detection (floor) and a table scene (table top), vertical planar patches (walls) for self localisation and edges reflecting transition between and boundaries of patches.

## 5 CONCLUSION AND OUTLOOK

In this paper we have presented a fast approach to segmentation of dense range images. In the first part of our approach mixed pixels at depth discontinuities in the range images are detected and masked out. The second part extracts step edges, roof edges as well as planar horizontal and vertical structures. We demonstrated that our approach is capable of real-time processing of range images on mainstream notebook hardware. Its computational

complexity is linear with the number of pixels of the input range images.

The test data used in this paper stemmed from a tilting laser range finder. Such a sensor is comparably slow and thus does not justify the use of fast algorithms. Therefore future work will focus on adjusting our algorithms to the specific sensor noise characteristics and geometry of the recently introduced and popular Kinect camera<sup>1</sup>. A second sensor of interest is a laser-based time-of-flight camera that is currently under development. It will deliver range images comparable to a tilting laser range finder but at frame rates of a camera [13].

## 6 ACKNOWLEDGEMENTS

The research leading to these results has received funding from the European Union's Seventh Framework Programme (FP7/2007-2013) under grant agreement n°248623.

## REFERENCES

- [1] Bellon O.R.P. and Silva L., New improvements to range image segmentation by edge detection. *Signal Processing Letters*, IEEE 9(2), 43–45, 2002.
- [2] Chang Y.L. and Li X., Adaptive image region-growing. *IEEE Transaction on Image Processing*, Vol. 3, pp. 868–872, 1994.
- [3] Gotardo P.F.U., Bellon O.R.P. and Silva L., Range image segmentation by surface extraction using an improved robust estimator. *IEEE Computer Society Conference on Computer Vision and Pattern Recognition*, Vol. 2. pp. II–33–8, 2003.
- [4] Haindl M. and Zid P., Multimodal Range Image Segmentation. *Vision Systems: Segmentation and Pattern Recognition*, Goro Obinata and Ashish Dutta (Ed.), ISBN: 978-3-902613-05-9, InTech, 2007.
- [5] Han F., Tu Z. and Zhu S.C., Range image segmentation by an effective jump-diffusion method. *IEEE Transactions on Pattern Analysis and Machine Intelligence*, 26(9), pp. 1138–1153, 2004.
- [6] Harati A., Gächter S. and Siegwart R., Fast Range Image Segmentation for Indoor 3D- SLAM. *6th IFAC Symposium on Intelligent Autonomous Vehicles*, IAV 2007, Toulouse, France, September 3–5, 2007.
- [7] Hijjatoleslami S.A. and Kittler J., Region growing: A new approach. *IEEE Transaction on Image Processing*, Vol. 7, pp. 1079–1084, 1998.
- [8] Hoover A., Jean-Baptiste G., Jiang X.Y., Flynn P.J., Bunke H., Goldof D.B., Bowyer K., Eggert D.W., Fitzgibbon A. and Fisher R.B., An Experimental Comparison of Range Image Segmentation Algorithms. *IEEE Trans. PAMI*, 18, no.7, pp. 673–689, 1996.

<sup>1</sup> <http://www.microsoft.com/en-us/kinectforwindows/>

- [9] Jiang X. and Bunke H., Fast segmentation of range images into planar regions by scan line grouping. *Machine Vision and Applications* 7(2), pp. 115–122, 1994.
- [10] Lee K.M., Meer P. and Park R.H., Robust Adaptive Segmentation of Range Images. *IEEE Transactions on Pattern Analysis and Machine Intelligence*, Vol. 20, No. 2, pp. 200–205, 1998.
- [11] Palmer P.L., Dabis H. and Kittler J., A performance measure for boundary detection algorithms. *Computer Vision and Image Understanding*, Vol. 63, pp. 476–494, 1996.
- [12] Sappa, A.D. and Devy M., Fast range image segmentation by an edge detection strategy. *Third International Conference on 3D Digital Imaging and Modelling*, pp. 292–299, 2001.
- [13] Thielemann, J.T., Sandner T., Schwarzer S., Cupcic U., Schumann-Olsen H. and Kirkhus T., TACO: A Three-dimensional Camera with Object Detection and Foveation. *Smarter sensors, easier processing - SAB 2010 workshops*, Paris, France, August 24, 2010.
- [14] Wang H. and Suter D., MDPE: A very robust estimator for model fitting and range image segmentation. *International Journal of Computer Vision* 59(2), pp. 139–166, 2004.
- [15] Weingarten J.W., Grüner G. and Siegwart R., Probabilistic plane fitting in 3D and an application to robotic mapping. *IEEE International Conference on Robotics and Automation*, Vol. 1. pp. 927–932, 2004.
- [16] Zhang X. and Zhao D., Range image segmentation via edges and critical points. *Proc. SPIE*, 2501, no. 3, pp. 1626–1637, 1995.



# COMPUTER AIDED DESIGN OF UNCONVENTIONAL BIO-ROBOTIC GRIPPER

Martin Jakubčík

Darina Kumičáková

Department of Automation and Production Systems, University of Zilina, Žilina, Slovakia

## ABSTRACT

In the case of non-traditional kinematic structure of the robot, respectively application of unconventional types of both actuators and transmission mechanisms in construction of their subsystems, it is necessary to look for new 3D modelling techniques which would provide the creation of virtual models with the required parameters. Construction of biorobotic gripper (BRG) is one of examples of such non-traditional structures. This one forms the end effector applicable to industrial and service robots. The use of BRG represents a highly innovative approach to the various manipulation tasks executing in framework of specialized applications and workspaces. The article presents approach to the 3D modelling of flexible elements that are active components of the finger virtual model actuating system. The structural variants of multi-fingered hand/BRG are described too.

Keywords: biorobotic gripper, pneumatic artificial muscles, flexible element 3D modelling

## 1 INTRODUCTION

Biorobotic hand (gripper) is multi-fingered hand (gripper) that is able to manipulate with objects of various shapes and dimensions in similar way as a human hand. There the term “multi-fingered hand” represents anthropomorphic concept of the design and the term “multi-fingered gripper” represents non-anthropomorphic one. The level of hand dexterity is evaluated on the base of its capability to manipulate with object by using rolling and sliding motions. Industrial gripper does not able to do it.

The present design concepts of robot hand/gripper construction are different. They have from three to five fingers that are arranged on the palm by different way. Every finger has three (or four) DOF most of all. The differences among the known concepts are in the used actuators and transmission systems too.

The Stanford/JPL Hand and MIT/Utah Hand represent a milestone for present multi-fingered robot hand concepts designing [7].

In this time the most known robot hands are: DLR Hand II and Karlsruhe Humanoid Hand (four-finger), Yaskawa Robot Hand (three-finger), Shadow Dexterous Hand C5 (five-finger), etc. The last mentioned one is actuated by air muscles through tendon transmission system.

Mechanism of bio-robot subsystem is usually specified with its construction and both un-conventional actuator and transmission systems too. Therefore the utilisation of CAx system suitable tools is of high importance. Verification of designed 3D model of mechanism by simulation requires the creation of the one as similar to expected real construction as it is most probably [1]. Created “real” 3D model is basis for the mechanism computer simulation. But the problem appears if the mechanism consists of flexible elements as artificial tendons, cables, air muscles, etc. These flexible elements can be understood:

- as a robot important accessory or
- as an active part of the driving mechanism.

In the first case, the one can be a cable kit of a robot welding torch that can come to the collisions with workplace’s components during the welding robot operating. The ineligible collisions states should be already identifiable during the robot simulation at the virtual workplace. But 3D modelling of the cable kits is a difficult problem because the one moves with the robot moving arm and due to its elasticity this one is bended three-dimensionally by various way. This is the actually solved

---

Contact authors: Martin Jakubčík<sup>1</sup>, Darina Kumičáková<sup>2</sup>

<sup>1</sup>Email: jakubcikm@fstroj.uniza.sk

<sup>2</sup>Email: darina.kumicakova@fstroj.uniza.sk

Univerzitná 1, 010 26 Žilina, SK-010 01 Slovak Republic

problem of worldwide producers of “off-line” programmes. The present approaches to this one are various. One of them is based on the cable kit alternate 3D models creating which consist of the cable kit specified critical areas only [6]. This approach was verified in CAD system SolidWorks (Dassault Systèmes SolidWorks Corp.) in framework of creation of methodology of the cable kits collision states identification by simulation. The obtained results enable to shift solution of this problem nearer to its real implementation into “off-line” programmes.

The second case we can connect with constructional concepts of robot hands/grippers where the transmission system consists of artificial tendons/flexible and inextensible cables and actuators represent by air muscles. The approach to 3D modelling of flexible elements of this type is solved as a partial problem in framework of forthcoming dissertation thesis “New Trends in Multi-fingered Robotic Grippers Designing” and is partially described below and in [4].

## 2 STRUCTURAL VARIANTS OF MULTI-FINGERED HAND

The idea to propose and manufacture a prototype of multi-fingered hand for educational and research purposes came into being at Department of Automation and Production Systems about six years ago. In regard of this fact the next initial baseline requirements were pre-set:

- the number of fingers equal to four ones,
- the ability to grasp objects of rotational and non-rotational shapes,
- easy design from viewpoint of its manufacturing and assembly too,
- utilisation of a principle of modularity in hand mechanical designing,
- utilisation of non-traditional actuators in driving system.

The first draft of multi-fingered hand design represents an anthropomorphic configuration of three identical fingers and one thumb (see Figure 2a). Kinematics of each finger (see Figure 1) consists of three links. The base joint has 2DOF and two next joints have 1 DOF separately. The distal links of fingers are actuated through rod passively. Kinematics of thumb consists of two links. This one is placed on the palm in opposition with fingers. The 1<sup>st</sup> variant of multi-fingered hand kinematic model had  $iH = 15$  DOF.

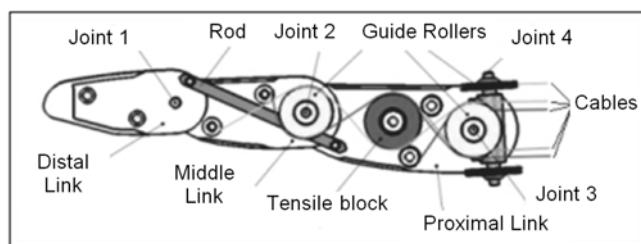


Figure 1 Structural design of the 1<sup>st</sup> finger's variant [8]

We can see that this finger's variant, in relation to its own dimensions, contains a large number of fitting parts. Because these facts would have result the complications of its production and assembly, the 1<sup>st</sup> variant of both finger and thumb designs were modified to enable:

- to reduce a number of the finger assembly components,
- to eliminate the finger assembly complexity,
- to extend the finger link internal space,
- to improve the elements stiffness and
- to produce the finger prototype with the suitable and available technology.

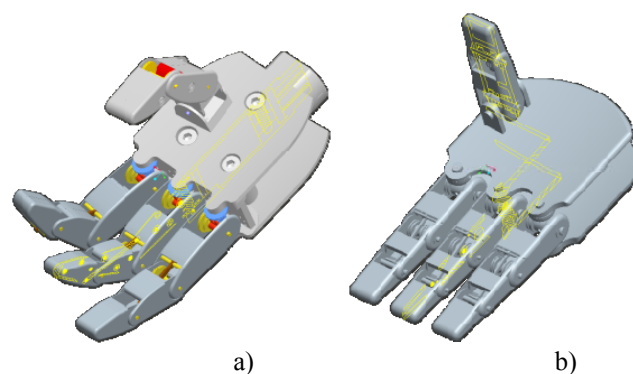


Figure 2 3D model of the multi-fingered hand  
a) the first variant [8],  
b) the second variant [9]

The result of these modifications had become the 2<sup>nd</sup> variant of the multi-fingered hand design (see Figure 2b) ready for production technology - Rapid Prototyping (RP). Construction adjustments are reflected in the next:

- simplifying of the both finger and thumb shapes,
- monolithic construction of the individual phalanges,
- separation of concentric pulleys and pins,
- enlargement of the model scale (about 2x).

In the next phase the prototype of one finger has been produced by fused deposition modelling technology with thermoplastic ABS 400, to test the finger links movement. Also was made a temporary basis to simulate a connection of the finger to the palm in the *metacarpophalangeal joint*. On this basis, we can test the functionality of a real finger prototype. We also verify the suitability of the artificial tendons (cables) used in the transmission system. These ones are stranded steel wires of small diameter that are used in the airplane pattern making routinely.

During the finger prototype assembly and its testing the following facts were found:

- the ratio of stiffness and flexibility of steel stranded wire that was applied in transmission system is sufficient because the leading cable copies surfaces of grooves in the pulleys during the motion (rotation) of phalanges to boundary positions;
- the problem occurred with the attachment of the end of the wire element to the shaped element made inside the phalange body. There is the lack of free space required for its final fixation;

- position of the steel wires outlet from the palm under proximal joint is not so optimal too. Primarily designed way causes the jumping-out of artificial tendons (cables) from the guide rollers and the finger prototype movement restriction. Another drawback accompanying this way of outlet is generation of additional torque on axis of the proximal joint.

Kinematic limitations detected during the functional analysis performed on the finger prototype showed the need of further modification and simplification of the biorobotic finger design.

The adjustment was based on creating of additional structural element and its connection with the fingers kinematic chain. This element - kind of "cradle" is joined with proximal link articularly and this one includes outlet for cable bowden and stranded wires. The cradle eliminates reaction forces from wires without restriction of movements of a finger. For the purposes of mounting trough bowden the internal shape of the proximal link has been changed too.

Thanks to these structural modifications the inner pulleys on the first joint was possible to remove.

On the basis of finger structure optimization it was possible to propose a new concept of biomechanical hand which takes account of the modified requirements for simplifying of the design and elimination of detected constructional drawbacks. This concept differs from the both earlier variants in its not so strict analogy with the human hand. Therefore further we will use the term "multi-fingered gripper" or "biorobotic gripper"- acronym "BRG", for this new structural concept.

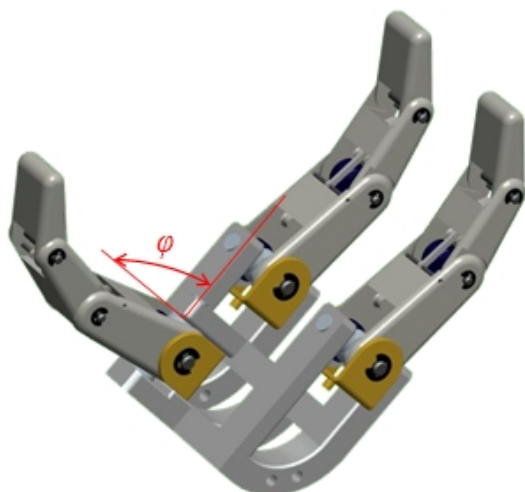


Figure 3 The third variant of BRG 3D model

The BRG concept is given by different number of fingers and their configuration at the palm. This one consists of three identical fingers of the same construction to reduce manufacturing costs. Two fingers are placed in the same row and the third one is in the opposite row – at angle  $\varphi$ =

90° (see Figure 3). Presented BRG has globally 12 degrees of freedom, of which 9 are actively controlled.

The subsystem of actuators for BRG actuating consists of air muscles, also called Pneumatic Artificial Muscles (PAMs). Their properties are currently most similar to the human muscles ones [7]. The PAMs are considered for the cables movement direct control. PAMs represents single-acting actuators. Therefore, the number of PAMs for the BRG depends on method of their interconnection. Generally, PAMs can be arranged in pairs antagonistically by two ways: PAM-PAM or PAM-Spring. This alternative arrangement means for BRG 3<sup>rd</sup> concept variant that the number of PAMs is  $N_{max} = 12$  and  $N_{min} = 6$ .



Figure 4 Virtual 3D model of finger design conception

The cables are fixed on the one side inside the phalanges and led through the internal space of every finger by the way similar to concept of the 1<sup>st</sup> variant but there the some modifications were done (see Figure 4). The cables are further led through the palm out to the gripper wrist. Because the palm of the 3<sup>rd</sup> concept variant is of new shape, the problem - "how the cables will be safely and without unacceptable collisions led inside this one?" will be solved yet. PAMs will be placed in the forearm zone. This way of BRG fingers actuation is called "remote actuation".

### 3 APPROACHES TO THE FLEXIBLE ELEMENTS 3D MODELLING

The basic problem of verification of the BRG 3<sup>rd</sup> design variant is creation of its real virtual model to simulate its activities in framework of real simulation in CAx system environment. The main problems results from:

- a large number of both degrees of freedom and members of the kinematic chain which movement must be controlled and
- flexible elements that are active elements of both transmission and actuating systems.

The finger structure is an open mechanism with serially linkage chain for which the physical parameters and their boundary conditions are not precisely defined. Therefore, the principle of bionics and heuristic approach based on empiricism and analogy with human hands will be used for the motion simulation.

The first phase of the flexible components simulation is focused on computer modelling of artificial tendons (wires) as the flexible elements which constitute the actuation and transmission mechanism of the BRG propulsion subsystem. However, at the present time no known CAD/CAE systems support the possibility of modelling such flexible bodies directly. Therefore, the idea of implementing the necessary simulations is to use Pro/Engineer WF5 and to apply alternative approaches to modelling and simulation mentioned flexible (shape-flexible) elements.

The base stage is to focus an attention to the analysis of solutions of the mechanical system and defining of the problems too. The concept of a flexible element as was presented in the context of a body (e.g., steel stranded wire) is characteristic of its flexibility and/or elasticity. Flexibility means a change of shape in a plane parallel to the largest dimension of the body without altering its volume.

Aiming at the simulation problem of 3D flexible cable in equipment operation simulation platform, the cable model is classified as two types which are named as:

- model of constant length and
- model of changeable length

Then two different simulation methods are put forward according to their respective 3D shape characteristics. Firstly, the catenary method is adopted to describe the model of constant length considering the gravity. The curve equation is deduced to be the final math model. Secondly, the model of changeable length is equal to draw a 3D line according two given 3D coordinate points and cylinder with certain radius around the line can be drawn with calling OpenGL API. The rendering effect of each model is presented to prove the simulation feasibility. Finally, the realization of mechanism called OpenGL call-back function combining with Vega is brought forward. It shows the greatest traits on the cable simulation in similar virtual reality system.

In this task we consider the cable as a 3D model with a constant length, resulting in the subsequent simulation procedures (chain method). Solution like this one represents the application of simulation based on object modelling features of the mechanism. The basic principle of testing is to simplify the real model to theoretical model, thus eliminating many parameters and variables entering into the process that affect the test results in ways previously unpredictable. Therefore, the BRG 3D model has been simplified to test the one. This is designed as a general mechanism of BRG subassembly containing only the elements directly coupled with the movement of the first wire. It means that the first phalange is connected with the base through the shaft to the pulley by the motion

constrain "User Defined - Pin" (defined as rotation around the axis).

Wire model is realized as a string created from the basic building element which is  $n$ -times inserted into the assembly and linked to the previous building element. Therefore, in the theoretical analysis we can conclude that if:

$n$  is number of elements of which the virtual 3D model of cable is composed, it can theoretically take values:

$$n(1, \infty),$$

$R$  is degree of similarity between both virtual and real models of wire expressed as a percentage of the fidelity model  $R(0, 100)$  and it is expressed in relation to  $n$  as:

$$R = f(n) \text{ and}$$

$dl$  is the length of the basic building element of wires and all elements have a constant length:  $dl_1 = dl_2 = \dots = dl_n$ , then  $l$  - total length of wire is expressed (1):

$$l = \sum_{i=1}^n dl_i \quad (1)$$

The basic building element of wire is modelled as a cylindrical body with given diameter which is closed from the one side by convex cylindrical surface and from the second side by concave surface. These both surfaces create references on the building elements for the mutual interconnection between every couple of elements in the chain. Fundamental element must include also coordinate planes and axes of cylindrical surfaces and coordinate points which are created at the intersection of the axes.

Trajectory of wire is defined by the cable outlet (output) at the base, a rotating guide roller surface and point of its mounting to the phalanges. This trajectory is created in the model as "Sketch" associative curve changing its shape depending on the position configuration of characteristic elements in their mutual movement.

Stranded wire is assembled as the virtual mechanism by using of motion constraint in "Assemble" module where each element of wire is connecting to the motion links "Pin-Axis Alignment" (alignment of axes of cylindrical surfaces) and "Slot - Point on Line" (alignment points and curve-trajectory) (see Figure 5). Characteristic of flexible bodies is their flexibility in a defined direction and a maximum value of bending. So these data are the boundary conditions for the simulation of their movement. Therefore, the angle of the axis rotation of two neighbouring elements in their link "Rotation Axis" is limited in the angle range  $\pm 70^\circ$ . To connect wire to the motion assembly, the first element is linked through the pivot to the phalange rotationally.

In context with the simulation of pneumatic artificial muscle (PAM) we must know its characteristics. This information is described together with a mathematical equation in [5] where the dependency between length  $L$  and diameter  $\varnothing d$  of PAM is expressed.

On the base of this mathematical relation the graphically simplified PUS parametric model is created in the form of a

cylinder. The length and diameter of the cylinder are defined by the function "Tools" and "Relations" as functions dependent on the control variable  $P$  which is determined and its value is changed by "Tools" "Parameters".

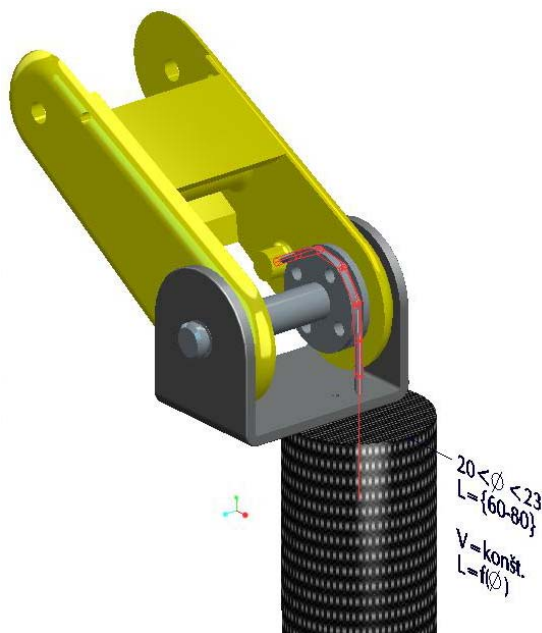


Figure 5 Simulation of the mechanism 3D virtual model with flexible elements (wire, PAM)

The proposed simulation model is possible to test in two ways. The first way is in the application "Mechanism" where the motion mechanism is created by inserting the actuator "Servomotor" to axis of the shaft and by defining its parameters (e.g. "Profile-Velocity", "Magnitude-Constant",  $A = \omega$ ). Through the function "Mechanism Analysis" we can create "Analysis Definition" which enables to show the behaviour of the simulated mechanism during its movement through "Playback", "Graph" functions. Another way is to connect the second end of wire ("assemble" of the last element) with simulation model of PAM. The length of the PAM will be changed with subsequent change in control parameter  $P$  and by regeneration of the model. It causes the tension of cable and rotational movement of the phalange.

The results of the simulations are following:

- in proportion to increasing number  $n$  of elements the difficulty and time of simulation calculations are increasing. It could be caused by system non-optimized calculation algorithm for a given application and hardware performance PC;
- simulation based on variations of parameter  $P$  enables to obtain only discrete values (angular rotation, position of elements) which provide only a little information in comparison with the method of "Mechanism" application.

The output of the present solutions should lead to the identification of size and speed of shortening of individual stranded wires by realization of predefined movements. These data may represent the important input parameters for control of pneumatic artificial muscles.

Another approach to the simulation of flexible elements consists of the linkage between the two methods described above. The cable model is classified as model of constant length, but isn't generated by the catenary method. A flexible element is formed by drawing a 3D spline, which is in coincidence with neutral fibre of cable. This spline is traced between two given 3D coordinate points. Real properties and parameters of cable determine the boundary conditions of spline (diameter, strain, curvature). This method is particularly suitable for example for simulation of the welding robot cable kits and their collisions during the robot motion in the framework of the welding workplace [6].

#### 4 FUTURE TASKS SPECIFICATION

At the present time a system that would enable to support comprehensive design solutions of the biorobotic gripper containing of flexible elements from the stage of its design to its test doesn't available for us. That is why our attention is aimed at the finding of suitable methodology for verification of this BRG virtual model design. The major task of the dissertation thesis is verification of the structural design and capability of biorobotic gripper in a suitable CAD/CAE system virtual environment.

Initial state of the topic and previously solved tasks are described in more detail in [2]. To this time we were able to propose the new variant of the BRG virtual model on which the possibility of simulation of flexible elements were tested. Now our task is to determine the kinematic relations and the impact of the forces acting on the flexible and coupled elements. In the next phase of the biorobotic gripper design verification is planned a virtual testing of the BRG grasping ability. For this purpose the objects of simple shapes called "shape primitives" (e.g. prism, cylinder, cone and sphere) will be used.

Contact model is characterised with forces that can be transmitted through the contact and allowed relative motions of two bodies in the contact area. These characteristics are determined by the geometry of contact surfaces and material properties of the parts that dictate friction and possible contact deformation. Various approaches to the analysis of manipulation, grasping and gripper are based on the rigid-body models where no deformation in contact points of two bodies is allowed. But these models are not able to describe the effect of contact completely. Compliant models are more complicated but they have several advantages [4]: they overcome the static indeterminacy inherent to rigid-body models and they predict the deformations of grasped or fixture parts during loading. A compliant contact deforms under the influence

of applied forces. The forces of interaction at the contact are derived from the compliance or stiffness model.

The main topic will be to create the suitable methodology for determining of the contact points among BRG fingers (and/or palm) and grasped object in CAE system environment. For this purpose the utilisation of function of program ProENGINEER (Creo Elements/Pro)-"Collision detection"- is considered.

The result of this effort should be led to the evaluation of the BRG 3rd variant grasping abilities with the goal to bring answers on the next questions:

- what types of objects can be grasped by this one ?
- is this one able to grasp a real assembly parts assembled in frame of automated laboratory workplace at our department ?

## 5 CONCLUSIONS

A common problem in the phase of the BRG design is verification and reviewing of correctness of the proposed variants of structures or modifications of the selected the 3rd concept variant in terms of its functionality. These testing of the BRG physical prototypes are time-consuming and expensive. The implementation of further design modifications is quite complicated.

Very progressive way is verification of the BRG design with application of both simulation and optimization methods. They are prepared as a computer program of CAE system on virtual model. Using the simulation system allows to engineers to determine operationally how the various selected kinematic and geometric parameters affect the monitored links abilities of proposed mechanism - for example: grasping objects of different shapes. In that manner it's possible to evaluate the functionality of the proposed prototype before its physical implementation phase and thus avoid the time, material and financial losses for non-optimal variant.

Note: This article was written thanks to the aid of project 054ŽU-4/2011 (K-11-004-00).

## REFERENCES

- [1] Daneshjo, N.: Chosen Methods and Techniques of Robot Systems Designing. *Habilitate work*. The Technical University of Košice, pp.77, 2008
- [2] Jakubčík, M. - Kumičáková, D.: Multi-functional robot hands. In: *11th International Scientific Conference „Automation in Production Planning and Manufacturing*. Žilina – Turčianske Teplice, Slovak Republic, ISBN 978-80-89276-23-3, pp. 116-121, 2010
- [3] Jakubčík, M.: Modeling strategies and simulation of biorobotics gripper motion transmission. In: *13th International Scientific Conference „Automation in Production Planning and Manufacturing*. Žilina – Turčianske Teplice, Slovak Republic, ISBN 978-80-89276-35-6, pp. 93-98, 2012
- [4] Kao, I.-Lynch, K.-Burdick, J.W.: Contact Modelling and Manipulation (Chapter 27.). In: *Handbook of Robotics*. Springer-Verlag Berlin Heidelberg, Editors: Siciliano, B, Khatib, O., pp. 1591, ISBN: 978-3-540-23957-4, 2008
- [5] Kolpach, S. - Kállay, F.: Research of McKibben pneumatic artificial muscle control. In: *ELEKTRO 2010 Proceedings of the 8th International Conference*. Žilina, Slovak Republic, ISBN 978-80-554-0196-6, pp 39-44, 2010
- [6] Kovačič, P.: The proposal of methodology of the collision states solving in frame of the welding robots "off-line" programming. *Dissertation thesis*, University of Žilina, Faculty of Mechanical Engineering, pp. 114, Žilina 2011
- [7] Melchiorri, C., Kaneko, M.: Robot Hands (Chapter 15.). In: *Handbook of Robotics*. Springer-Verlag Berlin Heidelberg, Editors: Siciliano, B, Khatib, O., pp. 1591, ISBN: 978-3-540-23957-4, 2008
- [8] Mužík, A.: Design of Biomechanical hand Virtual Model. *Diploma Work, VSPRM-255/2005, KOA, ŽU Žilina, pp. 100, 2005*
- [9] Zrniiová, L.: Verification of Constructional Design of Biomechanical Hand. *Diploma Work, VSPRM-283/2006, KOA, ŽU Žilina, pp. 64, 2006*

# INDUSTRIAL ROBOTS USED IN FORGES APPLICATIONS

Liviu Ciupitu\*

Andrei-Nick Ivanescu\*

Sorin Brotac\*\*

\* Politehnica University of Bucharest, Romania

\*\* S-Ind Process Control S.R.L., Bucharest, Romania

## ABSTRACT

Industrial robots are used especially in sectors where the human body is in danger or is working in extreme conditions. One of these sectors is the forges sector where the manipulating objects are hot, and the vibrations and noise are big. The problem of manipulation the hot parts implies the choosing of the right gripper mechanism in order to obtain the best cooling of it and of the robot itself. The cooling of gripper and robot is realized in the movement phase when no hot payload is present. In forge applications the temperatures of work pieces and of the environment are influencing the temperature of robot and the precision of it. The heat accumulated by the robot during a cycle depends to the temperature of work piece and to the time when the work piece is manipulated by the robot. So, the trajectory of movement is important and also the optimum position of robot with respect to the application positions is important. The proposed paper is dealing with the subject of moving the pose of base of robot with respect to the application poses so that an objective function representing the accumulated heat during a cycle to be minim.

Keywords: industrial robot, forge, optimum position

## 1 INTRODUCTION

Industrial robots are used especially in sectors where the human body is in danger or is working in extreme conditions. One of these sectors is the forges sector where the manipulating objects are hot, and the vibrations and noise are big. The problem of manipulation the hot parts implies firstly the choosing of the right gripper mechanism in order to obtain the best cooling of it and of the robot itself. In papers [9] and [10] grippers with 2 DOF are presented and could be used as well. But the position of robot with respect to the application, by taken into consideration the accumulated heat from work piece during the manipulation of it as an objective function, it is also a very important problem.

An empiric solution of determining the position of robot base on computing only the three coordinates of the origin of the Cartesian coordinate system assigned to the robot base is given in [7]. This empiric solution is not taken into consideration the way of moving of robot between the application poses but is taken into consideration the weight of object (tool) that the robot is moving between these. The proposed solution is not demonstrated by any mechanical and mathematical reasons.

In [11] an optimization problem of placement of a simple two-link planar manipulator by using a genetic algorithm is presented. Also in paper [8] a hybrid genetic algorithm is used in order to determine the optimum location of the base of robot with respect to imposed discrete positions of the end-effector.

The location of robot base with respect to the application is chosen so that all the interest point of application to be situated in the working space of robot. An optimization of this location by taken into consideration the minimum time of movement was presented in papers [1] and [6]. In paper [2] an optimum synthesis of motion law together with minimum time of motion was performed. In paper [4] the problem of optimal location of an industrial robot used in a forge application were formulated.

---

Contact author: Liviu Ciupitu

Faculty of Mechanical Engineering and Mechatronics,  
CG 018, Splaiul Independentei 313, sector 6, Bucuresti  
Email: liviu.ciupitu@omtr.pub.ro  
URL: <http://www.omtr.pub.ro/>

The mechanical structure of the industrial robot chosen by the manufacturers (for examples: Renault from France and Rahm from Italy), that are using it in forges sector, is of articulate kind with 6 DOF (Fig. 3). Sometime the opening area of forge makes difficult the inserting of hot part inside the forge even with 6 DOF. But an industrial robot with a mechanical structure of cylindrical type with at least 5 DOF (Fig. 4) may solve the problem too. Anyway the gripper used in such an application should have a special shape with long fingers made by special material heat resistant, in order to accumulate a minimum heat from manipulating part.

## 2 FORGING MANUFACTURING PROCESS

Usually the forged pieces are inserted from a bunker into a furnace in order to be heated (Fig. 1).

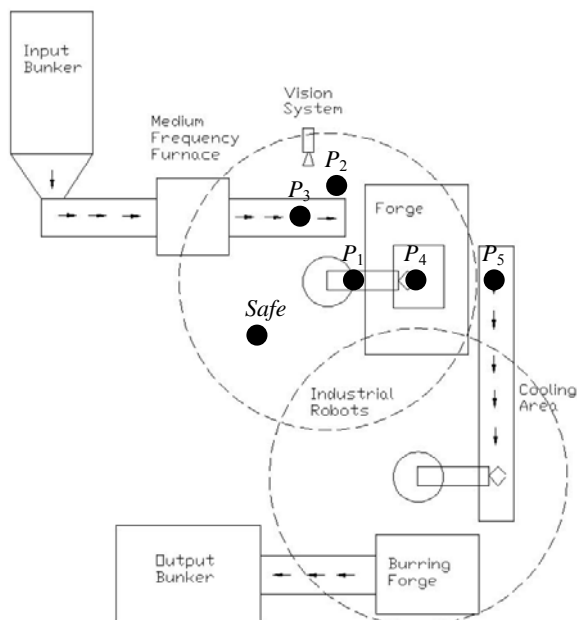


Figure 1 Application scheme

The hot part comes out from a medium frequency furnace with a random orientation or that can be fixed by special mechanisms, depending of the shape of part. But because of high temperature of part the individualization and orientation of part is difficult to be made with a good accuracy. So, a vision system to recognize the position of part and to communicate with the robot controller (Fig. 2) in order to make the position and orientation corrections of picking configuration, is necessary [3].

From delivering port of furnace the part is inserted by lateral into the forge and left down inside the forging mold. The inserting window is relatively small and requires a long link 6 of robot mechanisms (Fig. 3) or long gripper fingers.

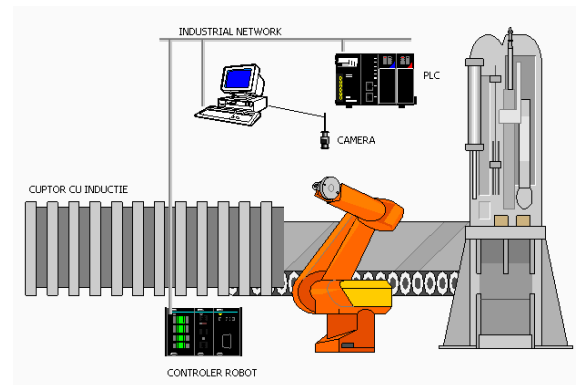


Figure 2 Communication scheme

Sometimes another task of spraying the parts of forge is done by the same robot with the aid of a special dose fixed to the robot arm or to the gripper. Anyway, the different planes in which the pick-and-place are done, and the small window of forge where the robot arm must be inserted, impose a 6 DOF spatial mechanism for robot mechanism (Fig. 3).

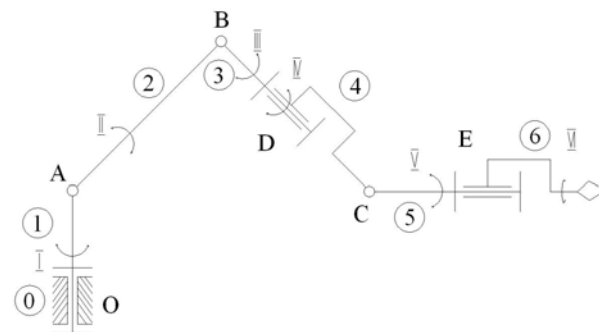


Figure 3 Articulated industrial robot with 6 DOF

An industrial robot with a mechanical structure of cylindrical type with at least 5 DOF (Fig. 4) may solve the problem too, but the prismatic joints are pretentiously even in case of cold manufacturing processes.

Actuating system is usual electric one for robot mechanism and pneumatic one for its gripper. The end-effector could be cooled by the aid of a fan or by pressure air in some situations when the temperature of manipulating part is high and the heat cannot be eliminated by the movement of the robot during one cycle.

The same inserting mode is used to put the work piece into the burring forge (Fig. 1). That can be done by another robot or by a human operator, but the work piece should be cold enough to not be deformed when the burring is done. So, a cooling area is interposed between main forge and burring forge, by using some fans. The transfer from main forge to the conveyer can be done by first robot or by the forge mechanism itself.

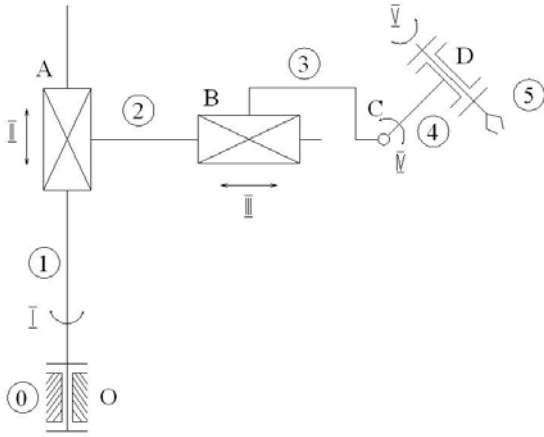


Figure 4 Cylindrical industrial robot with 5 DOF

Finally the forged piece is directed to another bunker and transported to another manufacturing cell.

### 3 OPTIMISATION

In order to formulate the optimization problem 2 models must to be known:

- the mechanical structure model of robot with minimum and maximum acceptable values for each joint independent parameter and
- the forge application model given by: poses that the robot must reach, the trajectories and motion laws between these points, the temperature of work pieces and the weight of them.

#### 3.1 ROBOT MECHANISM MODEL

Usual the mechanical structure model of a robot is implemented in robot controller by using Denavit-Hartenberg formalism [5] in order to find a transformation from tool tip to the base of robot. The matrix transformation of coordinates of a point  $P$  expressed in a  $O_{i+1}X_{i+1}Y_{i+1}Z_{i+1}$  coordinates system to coordinates of the same point in another  $O_iX_iY_iZ_i$  coordinates system is:

$$\mathbf{A}_i = \begin{bmatrix} 1 & 0 & 0 & 0 \\ a_i \cos \theta_i & \cos \theta_i & -\sin \theta_i \cos \alpha_i & \sin \theta_i \sin \alpha_i \\ a_i \sin \theta_i & \sin \theta_i & \cos \theta_i \cos \alpha_i & -\cos \theta_i \sin \alpha_i \\ s_i & 0 & \sin \alpha_i & \cos \alpha_i \end{bmatrix}$$

By choosing the axes systems in a special manner, the number of unknown parameters, between 2 Cartesian coordinates systems chosen anyway on each link, is reduced from six to four:

- 1)  $a_i$  - the length of common perpendicular measured from  $O_iZ_i$  axis to  $O_{i+1}Z_{i+1}$  axis;
- 2)  $s_i$  - the distance between  $O_iX_i$  and  $O_{i+1}X_{i+1}$  axes, measured upon  $O_iZ_i$  axis;

- 3)  $\alpha_i$  - angle between  $O_iZ_i$  and  $O_{i+1}Z_{i+1}$  axes, measured around  $X_{i+1}$  axis;

- 4)  $\theta_i$  - angle between  $O_iX_i$  and  $O_{i+1}X_{i+1}$  axes, measured around  $O_iZ_i$  axis.

For example for a serial robot mechanism with an open chain with 6 mobile links (Fig. 3), the coordinates transformation of a point  $P_j$  from  $O_7X_7Y_7Z_7$  axes system attached to the end-effector and it's the coordinates in base system  $O_1X_1Y_1Z_1$  could be write as follow [1]:

$$\begin{bmatrix} 1 \\ X_{1P_j} \\ Y_{1P_j} \\ Z_{1P_j} \end{bmatrix} = \mathbf{A}_1 \mathbf{A}_2 \mathbf{A}_3 \mathbf{A}_4 \mathbf{A}_5 \mathbf{A}_6 \begin{bmatrix} 1 \\ X_{7P_j} \\ Y_{7P_j} \\ Z_{7P_j} \end{bmatrix} \quad (1)$$

#### 3.2 FORGE APPLICATION MODEL

The model of forge application (Fig. 1) is simplified composed only by the 5 poses  $P_j$ ,  $j = \overline{1, 5}$ , that the robot must reach during the motion, without any obstacles defined (excluding the robot itself):

$P_1$  - in front of forge (waiting pose);

$P_2$  - upper of the picking pose;

$P_3$  - picking pose from the exit of furnace;

$P_4$  - pose of industrial robot inside forge;

$P_5$  - extreme pose of eliminating the piece from forge to the cooling on conveyer.

The motion from and to the *Safe* pose is made only one time at the beginning and, respectively, at the end of work.

Also the order of reaching these 5 poses in a complete cycle (i.e. for present case 8 intervals of motion:  $P_1 \rightarrow P_2 \rightarrow P_3 \rightarrow P_2 \rightarrow P_1 \rightarrow P_4 \rightarrow P_1 \rightarrow P_5 \rightarrow P_1$ ) and the motions laws between these are supposed as known. It is also possible that the orientation in one Cartesian position  $P_j(X_{0P_j}, Y_{0P_j}, Z_{0P_j})$  to be different depending the direction where the robot came from; in this case there will be teaches 2 different poses according to the needs of application.

Usual the robot controllers are implemented with only few motion laws between 2 poses from working space: of trapezoidal shape, of sinusoidal shape and of parabolic shape [12]. Transmission functions given numerically, and resulted for example from an optimization process done off-line [2], could be used for moving the end-effector of the robot along to a specific trajectory.

In forge applications, where the work pieces are hot, the temperatures of them and of the environment are influencing the temperature of robot and the precision of it. The heat accumulated by the robot during a cycle depends to the temperature of work piece and to the time when the work piece is manipulated by the robot. From 8 intervals of motions only in 4 of them the robot gripper is in contact with hot piece. On the other hand, during the manipulation, depending on the speed of robot, the robot gripper with the hot piece are cooling down by radiation heat transfer. The

robot gripper is cooling down in the other 4 intervals of motions, when the robot is not manipulating the hot piece, by radiation transfer of the heat accumulated when was in contact with hot piece.

Finally, especially for optimization problems that are dealing with forces and energy or power consumption, the weights  $G_{jk}$ ,  $j = \overline{1, 5}$ ,  $k = \overline{1, 5}$ , of objects moved by robots between application poses must to be known.

### 3.3 OPTIMIZATION PROBLEM

In order to start the formulation of optimization problem the unknown parameters must to be identified. The unknowns of optimization problem are the parameters that are defining the position and the orientation of Cartesian coordinates system assigned to the base of robot  $O_1X_1Y_1Z_1$  with respect to an inertial Cartesian system assigned to the "world of robot" (or to the application) denoted by  $O_0X_0Y_0Z_0$ . These parameters are composed by the 3 Cartesian coordinates of origin  $O_1$  expressed in Cartesian system  $O_0X_0Y_0Z_0$  ( $X_{0O_1}$ ,  $Y_{0O_1}$ ,  $Z_{0O_1}$ ) and by the 3 independent angles that are giving the orientation of Cartesian system assigned to the robot base  $O_1X_1Y_1Z_1$  with respect to Cartesian system  $O_0X_0Y_0Z_0$ , from the cosines directories matrix:

$$\mathbf{a}_{0,1} = \begin{pmatrix} \alpha_{X_0X_1} & \alpha_{X_0Y_1} & \alpha_{X_0Z_1} \\ \alpha_{Y_0X_1} & \alpha_{Y_0Y_1} & \alpha_{Y_0Z_1} \\ \alpha_{Z_0X_1} & \alpha_{Z_0Y_1} & \alpha_{Z_0Z_1} \end{pmatrix} \quad (2)$$

The number of unknown parameters could be reduced by choosing the Cartesian system  $O_0X_0Y_0Z_0$  in a Denavit-Hartenberg manner [5]. So, by choosing the  $O_0Z_0$  axis perpendicular to the  $O_1X_1$  axis (chosen randomly perpendicular to the  $O_1Z_1$  axis), results only 4 unknown parameters i.e. the Denavit-Hartenberg parameters :  $a_0$ ,  $s_0$ ,  $\alpha_0$ ,  $\theta_0$ . In this situation the coordinates of application points are constant with respect to the Cartesian system  $O_0X_0Y_0Z_0$  and the coordinates transformation equation is:

$$\begin{pmatrix} 1 \\ X_{0P_j} \\ Y_{0P_j} \\ Z_{0P_j} \end{pmatrix} = \mathbf{A}_0 \begin{pmatrix} 1 \\ X_{1P_j} \\ Y_{1P_j} \\ Z_{1P_j} \end{pmatrix} \quad (3)$$

The known parameters of optimization problem were formulated in previous paragraphs as follow:

- Denavit-Hartenberg parameters of mechanical structure of industrial robot with 6 DOF:  $a_i$ ,  $s_i$ ,  $\alpha_i$ ,  $\theta_i$ ,  $i = \overline{1, 6}$ ;
- poses of application with respect to  $O_0X_0Y_0Z_0$  Cartesian system which means the Cartesian coordinates of application points and the orientation matrices of end-

effector in these positions:  $X_{0P_j}$ ,  $Y_{0P_j}$ ,  $Z_{0P_j}$ ,  $\alpha_{0,7j}$ ,  $j = \overline{1, 5}$ ;

- trajectories between application points:  $T_{jk}$ ,  $j = \overline{1, 5}$ ,  $k = \overline{1, 5}$ ,  $j \neq k$ ;
- maximum speed and maximum acceleration accepted for each driving motor of robot joints:  $v_{i\max}$ ,  $a_{i\max}$ ,  $i = \overline{1, 6}$  and the other parameters of motions laws that are defining completely the transmission functions of first and second degree;
- temperatures of working piece during the manipulation of it:  $T_{32} \cong T_{21} \cong T_{14}$  and  $T_{45}$ ;
- weights of gripper and working piece during the manipulation sequence:  $G_{jk}$ ,  $j = \overline{1, 5}$ ,  $k = \overline{1, 5}$ ,  $j \neq k$ .

The objective function of optimization problem is a sum (or integral) of minimized parameter:

$$O = \sum_{l=1}^8 Q_l \quad (4)$$

where  $Q_l$  is the heat accumulated and/or lost by the robot in each interval of motion from a cycle:

$$Q_l = Q_{l, \text{cond}} - Q_{l, \text{conv}} \quad l = \overline{1, 8}.$$

The rate of heat transfer by conduction between two plane surfaces is given by the following relation:

$$\frac{Q_{\text{cond}}}{t} = \chi A \frac{T_{\text{hot\_piece}} - T_{\text{robot\_gripper}}}{d} \quad (5)$$

where:

$Q_{\text{cond}}$  is the heat transferred by conduction in time  $t$ ;

$\chi$  is the thermal conductivity of the barrier;

$A$  is area of contact surface;

$d$  is the thickness of barrier.

The heat lost by convection is given by the following relation:

$$Q_{\text{conv}} = \alpha A (T_{\text{robot}} - T_{\text{environment}}) \quad (6)$$

where:

$Q_{\text{conv}}$  is the heat lost by convection;

$\alpha$  is the thermal convection coefficient;

$A$  is area of convection surface.

The heat accumulated or lost by radiation transfer, between hot piece and environment and between robot and environment, is not taken into consideration in first approximation. Anyway the process of heat transfer between the hot piece and robot, between the hot piece and the environment and between robot and environment is very complex and it has to be approximated.

The process of finding the optimum set of parameters  $\{a_0^*$ ,  $s_0^*$ ,  $\alpha_0^*$ ,  $\theta_0^*\}$  is a numerical one where these parameters are changed during the computation according to a specific algorithm. At the beginning of computation, starting by an initial set  $\{a_0^{(0)}$ ,  $s_0^{(0)}$ ,  $\alpha_0^{(0)}$ ,  $\theta_0^{(0)}\}$ , a complete verification of application points  $P_j$ ,  $j = \overline{1, 5}$  so that to be into working space of robot is performed. This verification implies the computing of coordinates of all application points in  $O_1X_1Y_1Z_1$  Cartesian system:

$$\begin{pmatrix} 1 \\ X_{1P_j}^{(0)} \\ Y_{1P_j}^{(0)} \\ Z_{1P_j}^{(0)} \end{pmatrix} = \mathbf{A}_0^{-1} \begin{pmatrix} 1 \\ X_{0P_j} \\ Y_{0P_j} \\ Z_{0P_j} \end{pmatrix}, j = \overline{1, 5} \quad (7)$$

By inverse kinematics a set of joint independent variables  $\{\theta_{1,j}^{(0)}, \theta_{2,j}^{(0)}, \dots, \theta_{6,j}^{(0)}\}$  is determined for each pose  $(P_j, \alpha_{0,7j}), j = \overline{1, 5}$ .

A pose is in working space of robot if all independent variables values are between minimum and maximum acceptable values for each joint:

$$\theta_{i\min} \leq \theta_{i,j} \leq \theta_{i\max}, i = \overline{1, 6}, j = \overline{1, 5} \quad (8)$$

Conditions (8) represent the inequality constrains of optimization problem:

$$\theta_{i\min} - \theta_{i,j} \leq 0, i = \overline{1, 6}, j = \overline{1, 5} \quad (9)$$

$$\theta_{i,j} - \theta_{i\max} \leq 0, i = \overline{1, 6}, j = \overline{1, 5} \quad (10)$$

The inequality constrains (9) and (10) can be transformed in equality constrains:

$$h_k = \theta_{i\min} - \theta_{i,j} + w_k^2 = 0, i = \overline{1, 6}, j = \overline{1, 5} \quad (9')$$

$$h_{k+30} = \theta_{i,j} - \theta_{i\max} + w_{k+30}^2 = 0, k = \overline{1, 30} \quad (10')$$

by introducing the unknown parameters  $w_l$  where  $l = \overline{1, 60}$ .

The Lagrange method for solving of the minimization problems is based on transforming a given constrained minimization problem into an unconstrained minimization problem. This operation is accomplished by defining an appropriate auxiliary function, in terms of the problem functions, to define a new objective function whose minima is unconstrained in some domain of interest. The Lagrange function has the next form:

$$L = \mathbf{O} + \sum_{l=1}^{60} \lambda_l h_l \quad (11)$$

where  $\lambda_l, l = \overline{1, 60}$ , are Lagrange multipliers.

The necessary conditions for the minimizing the Lagrange function are:

$$\begin{aligned} \frac{\partial L}{\partial a_0} = 0, \frac{\partial L}{\partial s_0} = 0, \frac{\partial L}{\partial \alpha_0} = 0, \frac{\partial L}{\partial \theta_0} = 0, \\ \frac{\partial L}{\partial w_l} = 0, \frac{\partial L}{\partial \lambda_l} = 0, l = \overline{1, 60}. \end{aligned} \quad (12)$$

The non-linear system composed by 124 equations (12) with 124 unknowns is solved with a proper numerical method. The problem has infinity of solutions according to the initial solution.

## CONCLUSIONS

The optimum location of robot base depends to the robot structure and to the application. With same robot but different application positions and conditions results different locations for robot base.

The problem of finding the optimum location of robot base with respect to the application points according to an objective function is very important and could lead to major improvements [1], [8]. Sometimes the conditions of application impose special adjustments in order to protect the robot. The placing of robot base in an optimum location from the very first beginning is an essential initial task especially for large series productions. The economy of time or/and energy (money finally) for each product is decreasing it's price to almost a quarter [6] but the protection of industrial robot parts is much more important because without robot no production.

A multi-criteria optimisation, by taken into consideration the protection of industrial robot which is working in a hazardous environment and the economy of time and energy, is maybe the best approach.

## REFERENCES

- [1] Ciupitu L. and Simionescu I., Optimal Location of Robot Base With Respect to the Application Positions, Annals of DAAAM for 2007 & Proceedings of the 18<sup>th</sup> International DAAAM Symposium, ISBN 3-901509-58-5, ISSN 1726-9679, Editor B. Katalinic, Published by DAAAM International, Vienna, Austria, p.n. 82, pp. 161-162, 2007.
- [2] Ciupitu L., Simionescu I. and Ivanescu A.N., Optimum Synthesis of Motion Laws Used By Robot Controllers, Annals of DAAAM for 2008 & Proceedings of the 19<sup>th</sup> International DAAAM Symposium, ISBN 978-3-901509-68-1, ISSN 1726-9679, Editor B. Katalinic, Published by DAAAM International, Vienna, Austria, p.n. 141, pp. 0281-0282, 2008.
- [3] Ciupitu L., Brotac S. and Chivescu S., Optimum Position of an Industrial Robot Used in Forge Applications, Proceedings of the 4<sup>th</sup> International Conference on "Optimization of the Robots and Manipulators" OPTIROB 2009, Constanta-Mamaia, Romania, pp. 43-47, 2009.
- [4] Ciupitu, L. and A.N. Ivanescu. 2010. Optimal Location of an Industrial Robot used in Forge Applications, Annals of DAAAM for 2010 & Proceedings of the 21<sup>st</sup> International DAAAM Symposium, ISBN 978-3-901509-73-5, ISSN 1726-9679, Editor B. Katalinic, Published by DAAAM International, Vienna, Austria, p.n. 0227, pp. 0453-0455, 2010.

- [5] Denavit J. and Hartenberg R.S., A kinematic notation for lower-pair mechanisms based on matrices, *Trans ASME - J. Appl. Mech.*, 23, pp. 215–221, 1955.
- [6] Feddema, J.T. 1996. Kinematically optimal placement for minimum time coordinated motion, In: *Proceedings of the 1996 IEEE International Conference on Robotics and Automation*, Volume 4, 22-28 Apr 1996, Minneapolis, pp. 3395-3400, 1996.
- [7] Kovacs F. and Cojocaru G., *Manipulatoare, roboți și aplicațiile lor industriale*, Editura Facla, Timișoara, 1982.
- [8] Mitsi, S., Bouzakis K.D., Sagris D. and Mansour G., Determination of optimum robot base location considering discrete end-effector positions by means of hybrid genetic algorithm, *Robotics and Computer-Integrated Manufacturing*, 24 Elsevier Science, pp. 50-59, 2008.
- [9] Simionescu I. and Ciupitu L., Two Degrees of Freedom Grippers for Industrial Robots. *Proceedings of IX<sup>th</sup> International Conference on the Theory of Machines and Mechanisms*, Technical University of Liberec, Czech Republic, August 31-Sept. 2, ISBN 80-7083-847-7, pp. 711-716, 2004.
- [10] Simionescu I., Ciupitu L. and Ionescu C., Optimum Design of 2-DOF Robot Grippers, *Proceedings of the 3<sup>rd</sup> International Conference on "Optimization of the Robots and Manipulators" OPTIROB 2008*, Predeal, Romania, May 29<sup>th</sup>– June 1<sup>st</sup>, pp. 77-82, 2008.
- [11] Tian, L. and C. Collins. Optimal placement of a two-link planar manipulator using a genetic algorithm, *Robotica Journal*, Cambridge University Press, Issue 02 - Mar 2005, Volume 23, pp. 169-176, 2005.
- [12] \*\*\* (Intelitek Inc.), *Advanced Control Language for Controller-B, Reference Guide, Version F2.28, Catalog #100085 Rev. A*, 2003.

# HANDLING DEVICE DESIGN FOR GLASS PRODUCTS POSITIONING

Angela Javorová

Karol Velišek

Slovak University of Technology in Bratislava  
Faculty of Materials Science and Technology in Trnava  
Institute of Production Systems and Applied Mechanics  
Department of Technological Devices and Systems

## ABSTRACT

This paper deals with problems of manipulation with fragile semi products, types of grippers used for manipulation with them and their basics elements. Deployment of industrial robots and manipulators in the manufacturing is one of the biggest changes in recent decades in all industrial sectors. In this paper are solved designs of handling devices for positioning of diagonally cut glass products. Proposed solution was designed by CATIA system. This solution replaces the human operator with robot. The important automation process part is design of gripper for glass products handling.

Keywords: handling device, gripper, design process

## 1 INTRODUCTION

Industrial robots using fundamentally affects the humanization of human labour, human relieves stress and stereotyped from work activities. Human performance during working hours is fluctuating. This is due to physical and mental condition, his limited ability, such as easy vulnerability and low physical strength. Therefore, robotization of such operations is providing compensation primarily for human muscle strength of engine, which will increase the performance achieved. Replace human robots therefore delivers higher productivity, improved quality, product reliability and stability of production processes. [4] Industrial robots have to replace manual work in production especially in the automotive industry. The application of such assembly systems in practice is now the exception rather.

This is particularly suited of price follows a robot, especially in connection with the complexity and availability of sensor technology necessary for recognition and evaluation of robot part of technology. The general

structure of the robotic assembly systems are divided into three main groups:

- assembly systems where the robots perform only manipulation functions,
- assembly systems constituting the assembly center, where they are carried out in one place, manipulation, assembly and auxiliary functions,
- assembly systems, where the advanced generation assembly robot performs assembly and handling operations [3].

## 2 PROBLEM SOLVED

This paper describes how to design handling device for positioning glass semi products. Proposed handling device is designed to streamline the process of setting up of glass products to relieve cutting machine and operating workers performing this operation from hazardous work and stereotypical. In the present company is manufacturing machinery largely automated, but some workplaces are still reliant on human power. One of them is also part of the production line where workers manually based carafes to cutting machine. It is a process where the product is cutting at an angle. Product is the carafe with volume of 1500 ml Fig.1.

---

Contact author: Angela Javorová<sup>1</sup>

<sup>1</sup>Email: angela.javorova@stuba.sk



Figure 1 Product –glass carafe.

Cutting machine type designation BIEBUYCK-COMBI-12 is a device for cutting of glass products to a dimension which is required and also by grinding edges generated during cutting. Simplified model of the machine shown in Fig.2. The machine consists of twelve rotating clamping heads that rotate counter-clockwise around the central axis of the machine. The length of the machine cycle is in cutting operation is set to 5.5 s. The required operation is performed on the semi product in various positions during the said machine cycle.

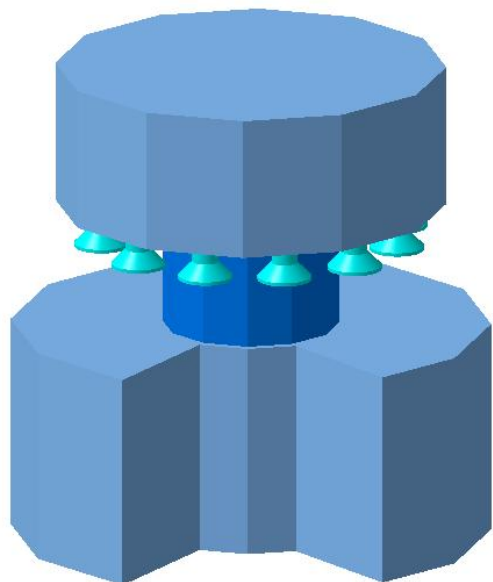


Figure 2 Simplified model of the cutting machine.

Clamping head (Fig. 3) together with the semi product clamped perform a rotational movement around its axis. Unwanted parts of carafe is cut and separated from the carafe during the rotation of the semi product and the resulting sharp edges are ground off. This process is carried out in 10 steps on the cutting machine. The first and last position of the 12-ers are designed for the creation of semi

products from the conveyor belt into the machine and unloading finished carafes from a machine on the conveyor belt.



Figure 3 Clamping heads of cutting machine.

The process of cutting, removing unwanted parts of the blanks is shown in Figure 4. Picture shows the method of semi product fixation in clamping heads by three jaws, which are made of nylon. Use nylon jaw prevents damage to the surface of the glass carafe which is prone to scratching.



Figure 4 Cutting process.

Manipulated object is a glass carafe with unwanted parts. This is a semi product of glass which after removal from the glass mold is transported by conveyor system, cooling furnace to cutting machine. Product goes to the final machining from the cutting machine on conveyor. Semi product (Fig.5) has a weight of 1.5 kg, height 390 mm and the diameter at its widest point  $\varnothing 228$  mm. This is inserted into the cutting machine by input manipulator.

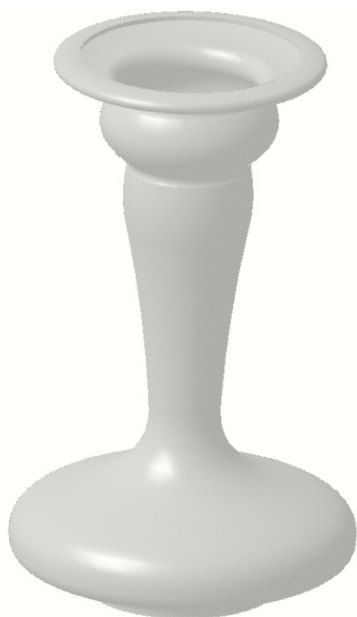


Figure 5 Semi product.

Trimmed carafe (Fig. 6) which is taken from the cutting machine weighs 0.902 kg and height 260 mm. Handling of the finished glass carafe provides an output manipulator.



Figure 6 Finished glass carafe.

### 3 DESIGN OF SINGLE-PURPOSE HANDLING DEVICE WITH SUCTION CUPS GRIPPER

Handling device (Fig. 7) was designed as a modular system composed of pneumatic linear and rotary actuators with a suction cups gripper. To solve of the handling operation was selected by two special purpose manipulators. The reason of this solution is modularity allowing design

handling devices for the type of material handling operations, with a simple kinematic structure, suitably selected drives and simple control by PLC [2]. Given the strong similarity of the handling operations of semi product insertion and product uploading from cutting machine are both handling devices identical. The difference is only in the setting of their drives and stoppers.

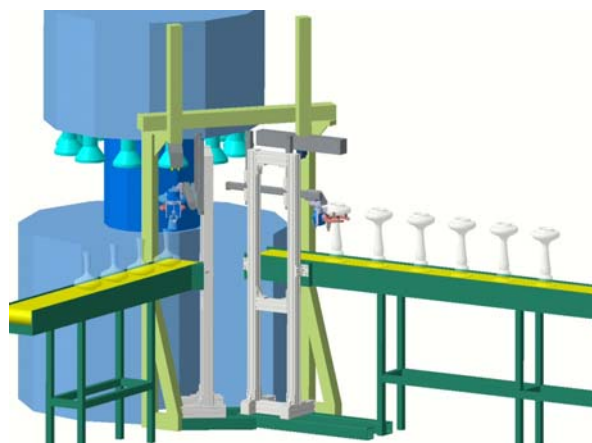


Figure 7 Model of link with integrated handling devices.

Designed handling device consist of these basic items:

- framework from aluminium profiles,
- two pneumatic linear actuators providing translational movement in the Z axis,
- linear actuator providing translational movement in Y axis,
- pneumatic rotary actuator performing a rotational movement in the Z axis,
- pneumatic rotary actuator performing a rotational movement in the Y axis,
- gripper.

Selection of individual components was based on the load (Table 1), which will affect them during positioning. Operating load values for each handling device component were calculated by summing the values of the weights of the components of mass effect on their load.

Table I

Components	Mass effect (kg)
Framework	19,694
Linear actuators in Z axis	12,614
Linear actuator in Y axis	6,416
Rotary actuator in Z axis	4,359
Rotary actuator in Y axis	2,447
Gripper	1,5

Handling devices framework was constructed of aluminium profiles FESTO HMBS 80/80, various sets of fasteners and caps. The framework model is in Figure 8.

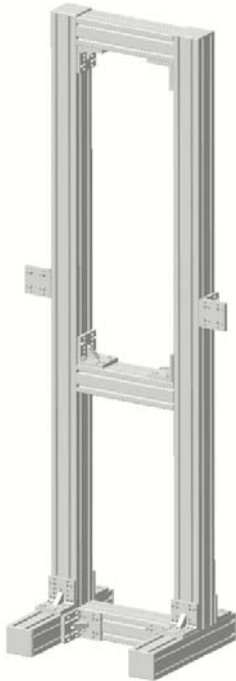


Figure 8 Handling devices framework constructed of aluminium profiles FESTO.

Framework was designed according to specific requirements for handling device workspace, load capacity and structural rigidity. The proposed structure is screwed on the conveyor belt (Fig. 9) for stability and precision re-established in the open position.

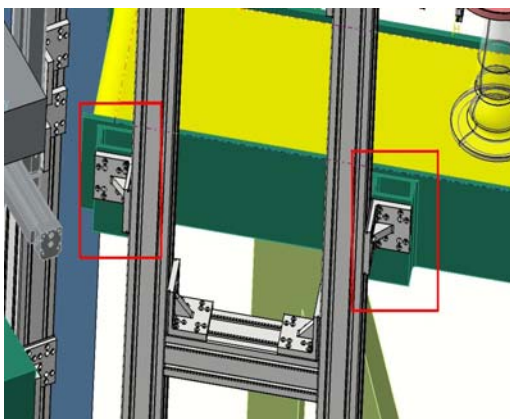


Figure 9 Connection framework of manipulation devices on conveyor belt by screws.

Pneumatics actuators combination is bolted to the framework construction by assembling clamps supplied with a connecting kit HMBV-ND-DL25. This combination consists of two linear and two rotary actuators. This actuators kinematics structures achieved required range of movements to insure handling operation.

Linear actuator performs handling object translational movement in Z and Y axis. Actuators selection was realized on the basic requirements. There are:

- desired range of motion,
- load,
- achieved speed of movement,
- end positions cushioning,
- assembly positioning,
- guide type,
- position sensing possibility,
- low weight of actuator,
- simply assembly,
- long lifetime.

Products company FESTO were selected from a wide range of drives offered in the market for material handling equipment. In the final stage of selection will be decided between electric and pneumatic drives. Given the lower weight of pneumatic actuators, easier control, the availability of compressed air supply and the extent of the use of pneumatic systems, it was decided to use pneumatic linear actuators in the proposed handling devices. Movement in the Z axis are provided by a pair of synchronized, vertically arranged pneumatic linear actuators DGPL-25-300-PPV-A-KF-B and Y axis movement ensures a horizontal stored pneumatic linear actuator DGPL-25-699-PPV-A-KF -B. Their layout and kinematics show figure10.

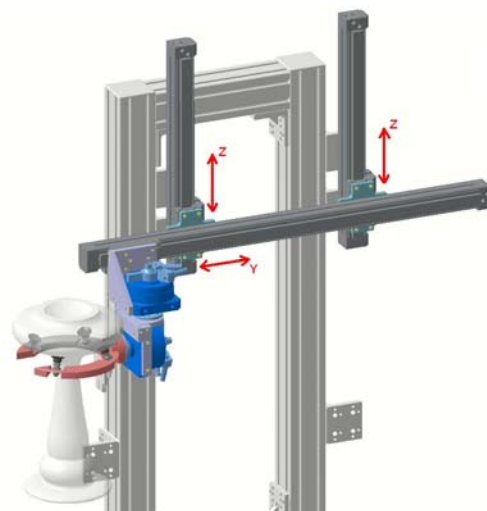


Figure 10 Linear actuators movements.

Linear actuator (Fig.11), provides sufficient speed and repeatable positioning accuracy to which the main impact of the use of ball guide in orbit packages. This guide performs relatively high load capacity.

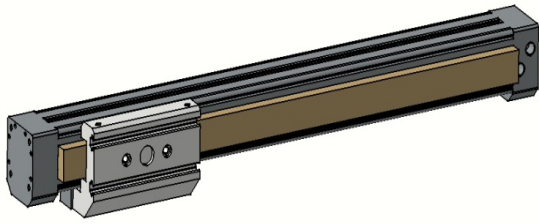


Figure 11 Linear pneumatic actuators FESTO typ DGPL-25-300-PPV-A-KF-B.

The role of rotary actuators is to ensure the desired angle of rotation and orientation direction of the manipulated object to cutting machine. The proposed device uses two such drives. Required movement characteristics of both drives were angle necessary in the rotation, in the first case, 180 degrees around the Z axis and the second 20 ° around the axis Y. Rotational movement in this axis is illustrated in Fig. 12.



Figure 12 Movements character of rotary actuators in different axes.

Double acting rotary actuators with swivel wing were selected. Double acting rotary actuators with swivel wing were selected. Rotary Actuator type designation DSM-32-270-P-FW-CC N was selected to implement a rotational movement at an angle of 180 degrees around the Z axis, on the basis of required parameters. 3D model of e selected drive is on Fig.13 The same type was chosen for rotational movement at an angle of 20 ° around the axis Y.

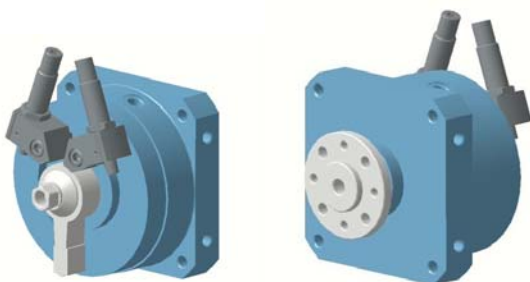


Figure 13 Swivel actuator model.

Gripping element of the proposed handling devices is gripping head with suction cups (Fig.14).



Figure 14 Model vacuum gripper.

This type manipulated object grasping ensures a sufficient gripping force and gripping stability. Using suction cups, which contact surface is made of soft material does not damage the surface of the manipulated object. This is a great advantage compared to mechanical gripper with jaws, which is difficult to ensure sufficient grasp power for safe positioning and taking into account the fragility of the manipulated object. [1]. Gripper was designed to specific requirements of grasping the semi product. There are:

- semi product fragility,
- semi product smooth surface,
- tendency to scratch the surface,
- grip precision,
- sufficient gripping power,
- semi product dimensions.

Additional requirements needed to gripping head:

- low weight,
- ease of construction,
- resistance to environmental,
- structural rigidity,
- easy manufacturability.

The basic structural part of gripping head is ring, which is made of aluminium alloy 4201 42 by cutting operation on CNC milling machines. The material was selected for its low weight, strength, ease of machinability and corrosion resistance. The resulting shape of the ring is shown by the 3D model of Fig.15.



Figure 15 Model of gripper ring.

Contact gripping head with the manipulated object is realized by suction cups, which ensure sufficient grasp power, necessary for rapid and safe handling. The main requirements that have been asked to sucker in their choice:

- grasp stability,
- precision grip,
- suitability of materials suckers,
- lifetime,
- grip power,
- angle and height compensator,
- simple installation,
- low weight of individual components.

To facilitate the selection of the appropriate type and number of cups was used to design software FESTO Vacuum Selection. Suction cups with the type designation ESG-30-SN-CK-HC-F-WA (Fig.16) were selected.



Figure 16 Suction cup model.

Have the following parameters:

- diameter of the suckers -  $\varnothing 30$  mm,
- suction cup shape – standard,
- suction cup material - Perbunan (NBR),
- tear strength at -0.7 bar - 40.8 N,
- suction cup capacity -  $0.867 \text{ cm}^3$ ,
- mount - type HC,
- weight - 42 g.

Suitable type of suction nozzle VADMI 45-LS-N was chosen on the basis of the cups. This suction nozzle is based the Venturi principle and used to create the vacuum necessary for powered suction cups. The nozzle is equipped with an integrated solenoid valve for outlet air mechanism, involving the savings for the air filter and an indication of an integrated silencer. Suction nozzle parameters are:

- operating pressure - 2 to 8 bar,
- temperature range - from  $0^\circ \text{C}$  to  $60^\circ \text{C}$ ,
- nominal width - 0.45 mm,
- protection - IP65,
- weight - 90 g.

Gripper is attached to the swivel drive means of a coupling flange (Fig.17). Semi product to manufacture flanges was chosen rod  $\varnothing 63$  mm circular cross section of aluminum alloy 42 4,201th.

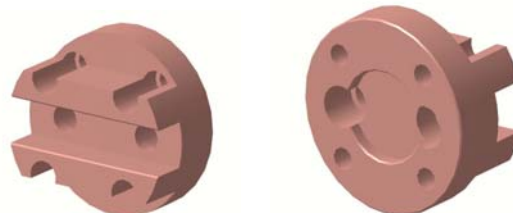


Figure 17 Coupling flange.

## CONCLUSION

A problem of design and application handling equipment to the manufacturing process is very complex and extensive. One of the key means for development of engineering industry is a complex automation, which affects all industries. Automation solves complex problems such as manufacturing and non-manufacturing sector.

## REFERENCES

- [1] Palko A., Smrček J., *Robotika-koncové efekторыpre priemyselné aservisné roboty*. 1st edition, Košice: Edícia vedeckej a odbornej literatúry, 2004.
- [2] Matička R., Talácko J., *Mechanismy manipulátoru a prumyslových robotu*. 1st edition, Praha, 1991.
- [3] Hrušková E., Holubek R., Increasing of effectiveness of manufacturing and directing technical level. *Proceedings in Manufacturing Systems*, Vol. 5, No 4, pp. 203-208, 2010.
- [4] Holubek R., Vlášek M., Košťál P., Clamping jaws with sensory equipment for intelligent fixture. *Annals of DAAAM for 2010 & Proceedings of the 21st International DAAAM Symposium*, Vol. 21, No 1, pp. 1173-1174, 2010.

# TEMPLATE FOR PREPARING PAPERS FOR PUBLISHING IN INTERNATIONAL JOURNAL OF MECHANICS AND CONTROL

Author1\*      Author2\*\*

\* affiliation Author1

\*\* affiliation Author2

## ABSTRACT

This is a brief guide to prepare papers in a better style for publishing in International Journal of Mechanics and Control (JoMaC). It gives details of the preferred style in a template format to ease paper presentation. The abstract must be able to indicate the principal authors' contribution to the argument containing the chosen method and the obtained results. (max 200 words)

Keywords: keywords list (max 5 words)

## 1 TITLE OF SECTION (E.G. INTRODUCTION)

This sample article is to show you how to prepare papers in a standard style for publishing in International Journal of Mechanics and Control.

It offers you a template for paper layout, and describes points you should notice before you submit your papers.

## 2 PREPARATION OF PAPERS

### 2.1 SUBMISSION OF PAPERS

The papers should be submitted in the form of an electronic document, either in Microsoft Word format (Word'97 version or earlier).

In addition to the electronic version a hardcopy of the complete paper including diagrams with annotations must be supplied. The final format of the papers will be A4 page size with a two column layout. The text will be Times New Roman font size 10.

## 2.2 DETAILS OF PAPER LAYOUT

### 2.2.1 Style of Writing

The language is English and with UK/European spelling. The papers should be written in the third person. Related work conducted elsewhere may be criticised but not the individuals conducting the work. The paper should be comprehensible both to specialists in the appropriate field and to those with a general understanding of the subject. Company names or advertising, direct or indirect, is not permitted and product names will only be included at the discretion of the editor. Abbreviations should be spelt out in full the first time they appear and their abbreviated form included in brackets immediately after. Words used in a special context should appear in inverted single quotation mark the first time they appear. Papers are accepted also on the basis that they may be edited for style and language.

### 2.2.2 Paper length

Paper length is free, but should normally not exceed 10000 words and twenty illustrations.

### 2.2.3 Diagrams and figures

Figures and Tables will either be entered in one column or two columns and should be 80 mm or 160 mm wide respectively. A minimum line width of 1 point is required at actual size. Captions and annotations should be in 10 point with the first letter only capitalised *at actual size* (see Figure 1 and Table VII).

---

Contact author: author1<sup>1</sup>, author2<sup>2</sup>

<sup>1</sup>Address of author1.

<sup>2</sup>Address of author2 if different from author1's address  
E-mail: author1@univ1.com , author2@univ2.com

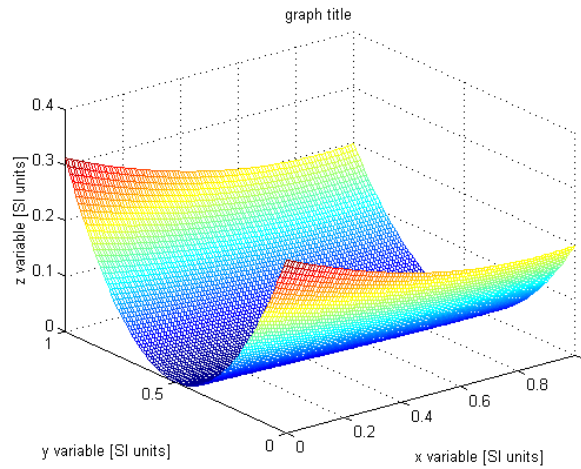


Figure 1 Simple chart.

Table VII - Experimental values

Robot Arm Velocity (rad/s)	Motor Torque (Nm)
0.123	10.123
1.456	20.234
2.789	30.345
3.012	40.456

#### 2.2.4 Photographs and illustrations

Authors could wish to publish in full colour photographs and illustrations. Photographs and illustrations should be included in the electronic document and a copy of their original sent. Illustrations in full colour ...

#### 2.2.5 Equations

Each equation should occur on a new line with uniform spacing from adjacent text as indicated in this template. The equations, where they are referred to in the text, should be numbered sequentially and their identifier enclosed in parenthesis, right justified. The symbols, where referred to in the text, should be italicised.

- point 1
  - point 2
    - point 3
- 1. numbered point 1
- 2. numbered point 2
- 3. numbered point 3

$$W(d) = G(A_0, \sigma, d) = \frac{1}{T} \int_0^{+\infty} A_0 \cdot e^{-\frac{d^2}{2\sigma^2}} dt \quad (1)$$

### 3 COPYRIGHT

Authors will be asked to sign a copyright transfer form prior to JoMaC publishing of their paper. Reproduction of any part of the publication is not allowed elsewhere without permission from JoMaC whose prior publication must be cited. The understanding is that they have been neither previously published nor submitted concurrently to any other publisher.

### 4 PEER REVIEW

Papers for publication in JoMaC will first undergo review by anonymous, impartial specialists in the appropriate field. Based on the comments of the referees the Editor will decide on acceptance, revision or rejection. The authors will be provided with copies of the reviewers' remarks to aid in revision and improvement where appropriate.

### 5 REFERENCES (DESCRIPTION)

The papers in the reference list must be cited in the text. In the text the citation should appear in square brackets [ ], as in, for example, "the red fox has been shown to jump the black cat [3] but not when...". In the Reference list the font should be Times New Roman with 10 point size. Author's first names should be terminated by a 'full stop'. The reference number should be enclosed in brackets. The book titles should be in *italics*, followed by a 'full stop'. Proceedings or journal titles should be in *italics*. For instance:

#### REFERENCES (EXAMPLE)

- [1] Smith J., Jones A.B. and Brown J., *The title of the book*. 1st edition, Publisher, 2001.
- [2] Smith J., Jones A.B. and Brown J., The title of the paper. *Proc. of Conference Name*, where it took place, Vol. 1, paper number, pp. 1-11, 2001.
- [3] Smith J., Jones A.B. and Brown J., The title of the paper. *Journal Name*, Vol. 1, No. 1, pp. 1-11, 2001.
- [4] Smith J., Jones A.B. and Brown J., *Patent title*, U.S. Patent number, 2001.

*International Journal of Mechanics and Control – JoMaC*  
Published by Levrotto&Bella  
**TRANSFER OF COPYRIGHT AGREEMENT**

<p>NOTE: Authors/copyright holders are asked to complete this form signing section A, B or C and mail it to the editor office with the manuscript or as soon afterwards as possible.</p>	<p><i>Editor's office address:</i> Andrea Manuello Bertetto Elvio Bonisoli <i>Dept. of Mechanics</i> <i>Technical University – Politecnico di Torino</i> <i>C.so Duca degli Abruzzi, 24 – 10129 Torino – Italy</i> <i>e_mail: jomac@polito.it</i> <i>fax n.: +39.011.564.6999</i></p>
--	---

The article title:

---

By: \_\_\_\_\_

To be Published in *International Journal of Mechanics and Control JoMaC*  
*Official legal Turin court registration Number 5320 (5 May 2000) - reg. Tribunale di Torino N. 5390 del 5 maggio 2000*

- A Copyright to the above article is hereby transferred to the JoMaC, effective upon acceptance for publication. However the following rights are reserved by the author(s)/copyright holder(s):
1. All proprietary rights other than copyright, such as patent rights;
  2. The right to use, free or charge, all or part of this article in future works of their own, such as books and lectures;
  3. The right to reproduce the article for their own purposes provided the copies are not offered for sale.
- To be signed below by all authors or, if signed by only one author on behalf of all co-authors, the statement A2 below must be signed.*

A1. All authors:

SIGNATURE \_\_\_\_\_ DATE \_\_\_\_\_ SIGNATURE \_\_\_\_\_ DATE \_\_\_\_\_

PRINTED NAME \_\_\_\_\_ PRINTED NAME \_\_\_\_\_

SIGNATURE \_\_\_\_\_ DATE \_\_\_\_\_ SIGNATURE \_\_\_\_\_ DATE \_\_\_\_\_

PRINTED NAME \_\_\_\_\_ PRINTED NAME \_\_\_\_\_

A2. One author on behalf of all co-authors:

*"I represent and warrant that I am authorised to execute this transfer of copyright on behalf of all the authors of the article referred to above"*

PRINTED NAME \_\_\_\_\_

SIGNATURE \_\_\_\_\_ TITLE \_\_\_\_\_ DATE \_\_\_\_\_

B. The above article was written as part of duties as an employee or otherwise as a work made for hire. As an authorised representative of the employer or other proprietor. I hereby transfer copyright to the above article to *International Journal of Mechanics and Control* effective upon publication. However, the following rights are reserved:

1. All proprietary rights other than copyright, such as patent rights;
2. The right to use, free or charge, all or part of this article in future works of their own, such as books and lectures;
3. The right to reproduce the article for their own purposes provided the copies are not offered for sale.

PRINTED NAME \_\_\_\_\_

SIGNATURE \_\_\_\_\_ TITLE \_\_\_\_\_ DATE \_\_\_\_\_

C. I certify that the above article has been written in the course of employment by the United States Government so that no copyright exists, or by the United Kingdom Government (Crown Copyright), thus there is no transfer of copyright.

PRINTED NAME \_\_\_\_\_

SIGNATURE \_\_\_\_\_ TITLE \_\_\_\_\_ DATE \_\_\_\_\_

## CONTENTS

- 3 A PTZ Stereo Camera Vision System for Robotic Perception**  
*G. Macesanu, S.M. Grigorescu, F. Moldoveanu*
- 9 Mechanical Harvester and Double Flow Cyclone Separator: Prototypes to Improve Saffron Spice Productions**  
*A. Manuello Bertetto, R. Ricciu*
- 15 Evolutionary Algorithm to Solve the Trajectory Planning Problem, with Robot Dynamics Considerations**  
*F.J. Abu-Dakka, F. Valero, J.L. Suñer, V. Mata*
- 21 Fast Range Image Segmentation for a Domestic Service Robot**  
*P. Einramhof, R. Schwarz, M. Vincze*
- 29 Computer Aided Design of Unconventional Bio-Robotic Gripper**  
*M. Jakubčík, D. Kumičáková*
- 35 Industrial Robots Used in Forges Applications**  
*L. Ciupitu, A.N. Ivanescu, S. Brotac*
- 41 Handling Device Design for Glass Products Positioning**  
*A. Javorová, K. Velišek*

### *next number scheduled titles:*

Epi.q-1.2, A Hybrid Mobile Mini Robot with a Reconfigurable Three Wheeled Locomotion Unit  
*G. Quaglia, W. Franco, D. Maffiodo, S. Appendino and R. Oderio*

Modelling and Temperature Control of Shape Memory Alloys with Fast Electrical Heating  
*R. Velázquez and E.E. Pissaloux*

Vehicles Headlamps Glare Effect Removal  
*G. Ligios and A. Manuello Bertetto*

Nonlinear Elastic Characteristic of Magnetic Suspensions through Hilbert Transform  
*E. Bonisoli*

The Mechanism of Crank Initiation and Propagation in Metallic Engineering Materials  
*V.T. Hoang*